Metal Template Synthesis of 'Broken' Aromatic Preorganized Terdentate Hosts for the Recognition of Lanthanide Tris-β-Diketonate Guests

Le, Hoang Giau; Guenee, Laure; Naseri, Soroush; Besnard, Céline; Piguet, Claude

How to cite

LE, Hoang Giau et al. Metal Template Synthesis of 'Broken' Aromatic Preorganized Terdentate Hosts for the Recognition of Lanthanide Tris-β-Diketonate Guests. In: Helvetica chimica acta, 2023, p. e202200190. doi: 10.1002/hlca.202200190

This publication URL: https://archive-ouverte.unige.ch/unige:168337
Publication DOI: 10.1002/hlca.202200190

doi.org/10.1002/hlca.202200190

RESEARCH ARTICLE

HELVETICA chimica acta

Metal Template Synthesis of 'Broken' Aromatic Preorganized Terdentate Hosts for the Recognition of Lanthanide Tris-β-Diketonate Guests

Giau Le-Hoang,*[a] Laure Guénée,[b] Soroush Naseri,[a] Céline Besnard,[b] and Claude Piguet*[a]

[a] Department of Inorganic and Analytical Chemistry, University of Geneva, 30 quai E. Ansermet, CH-1211 Geneva 4, Switzerland, e-mail: Claude.Piguet@unige.ch; Hoang.Le@unige.ch

[b] Laboratory of Crystallography, University of Geneva, 24 quai E. Ansermet, CH-1211 Geneva 4, Switzerland

Dedicated to Professor *Robert Deschenaux* in tribute to his unfailing support and friendship

The binding of the terdentate precursor 2,2′-(4-methyl-3,5-divinylpyridine-2,6-diyl)bis(1-allyl-5-bromo-1*H*-benzo[*d*]imidazole) (**1**) to the lanthanide container [Ln(hfac)$_3$] (Ln=La, Eu, Gd, Y, Er; H-hfac = 1,1,1,5,5,5-hexafluoropentane-2,4-dione) ensures the *cis-cis* orientation of the two adjacent α,α′-diimine units that is required for the successful intramolecular *Grubb* ring-closing metathesis generating the target rigid 6-methyl-9,11-dihydro-1*H*,3*H*-2λ^2,10λ^2-pyrido[2,3-*c*:6,5-*c*′]bis(azepine) scaffold decorated with two terminal 5-bromo-1*H*-benzo[*d*]imidazole in ligand **L7**. The bond valence analysis of the crystal structures of the associated nine-coordinate adducts [**L7**Ln(hfac)$_3$] (Ln=La, Eu, Gd, Er, Y) reveals a satisfying match between the rigid terdentate cavity and the size of the bound lanthanide metal, with a pronounced preference for the largest lanthanum cation. Thermodynamic studies in dichloromethane confirm the formation of [**L7**Ln(hfac)$_3$] adducts with unprecedented stabilities due to the removal of the energy penalty associated with *trans-trans* to *cis-cis* reorganization. The introduction of saturated methylene groups within the polyaromatic ligand backbone breaks extended aromatic delocalization and clears the visible part of the electromagnetic spectrum from emission arising from low-energy ligand-based excited states.

Keywords: Lanthanides, template synthesis, ring-closing metathesis, preorganization, heteroleptic complexes.

Introduction

During the last two decades, lanthanide-based complexes [**L**$_m$Ln$_n$] have found widespread applications as therapeutic agents,[1,2] catalysts,[3] luminescent bioprobes[4,5] and templating agents for sophisticated (supra)molecular architectures,[6,7] just to name a few. Their thermodynamic formation constants $\beta_{m,n}^{\mathbf{L},\mathrm{Ln}}$ mainly depend on *1*) the size of the trivalent lanthanide ions (Ln), a parameter that can be selected along the series, and *2*) the nature of the ligand (**L**), which corresponds to the main aspect explored by chemists for the rational tuning of its affinity for the entering metal.[8–11] For a given ligand with specific structural and electronic properties (size of the chelating ring, nature and arrangement of the donor atoms, denticity, *etc.*), the dependence of the formation constant on the lanthanide size along series is often monotonic with either positive or negative slopes, but significant deviations are regularly reported showing convex or concave bowl-shape trends.[9,10,12–14] As an example, the affinity of ligand **L1** for [Ln(hfac)$_3$] containers in acetonitrile displays a global decrease along the series, yet modulated by some bowl-shape selectivity for mid-range lanthanides (*Figure 1,b*).[12] On the other hand, the associated stability constants of the given lanthanum complexes [**L*k***La(hfac)$_3$] (**L*k*** = **L1**–**L2**) decreases when

Supporting information for this article is available on the WWW under https://doi.org/10.1002/hlca.202200190

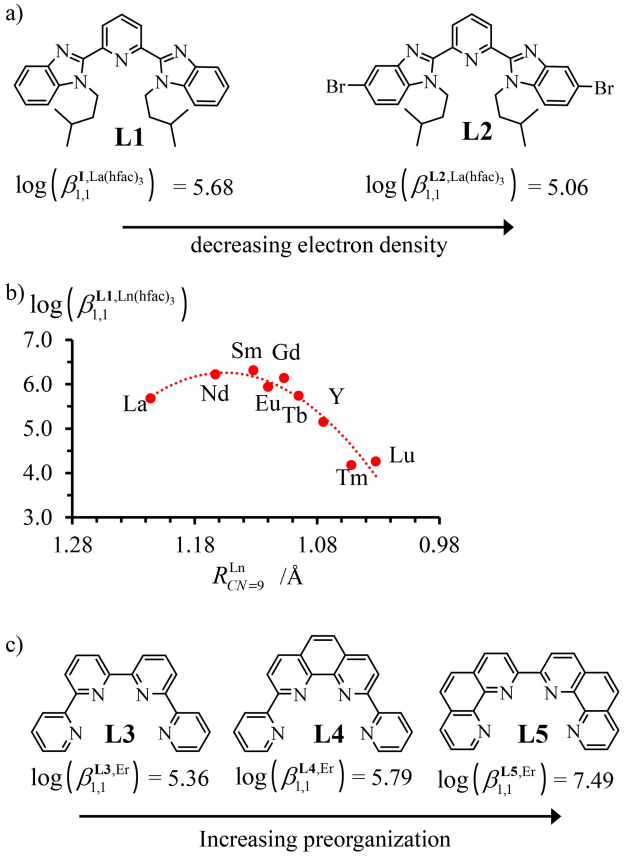

Figure 1. Effects of a) electronic density and b) lanthanide size on the thermodynamic formation constants of the adduct [**Lk**Ln(hfac)$_3$] in CH_3CN (**Lk** = **L1**, **L2**; 298 K),[12] and c) structural preorganization on the stability constants of the lanthanide complexes [**Lk**Er]$^{3+}$ measured in 50% CH_3OH/H_2O (**Lk** = **L3**–**L5**, 298 K).[15]

electron-withdrawing groups (Br-atoms in **L2**) are connected to the benzimidazole rings found in ligand **L1** (*Figure 1,a*).[12] It has also been noticed that the stabilities of the resulting lanthanide complexes may be further maximized when using the concept of preorganization.[16] In this context, the increased level of preorganization programmed along the **L3**→**L4**→**L5** series of polyaromatic ligands (*Figure 1,c*) results in a significant thermodynamic stabilization: a trend assigned to the stepwise removal of energy penalty induced by the *cis-cis*→*trans-trans* rearrangement required for complexing the α,α′-diimine binding units to the lanthanide ions.[15,17–19] However, rigidification to give highly preorganized ligands often relies on extended polyaromatic backbones, which *1*) affects the excited electronic levels used for sensitizing trivalent lanthanides in light-converting devices[20] and *2*) sometimes prevents the design of cavities adapted for the complexation of the smaller trivalent lanthanides.[15,19] Associated with the chelate effect, some partial polyaromatic preorganization is yet sufficient for inducing selective extraction processes, and semi-rigid polydentate heterocyclic *N*-donor ligands have been systematically exploited for the selective complexation of larger (and softer) trivalent actinides over related smaller (and harder) lanthanides upon nuclear waste treatments.[21–26]

Preorganization beyond simple rigid polyaromatic scaffolds usually exploits metal-templated synthesis in order to assemble and dispose the bound units into favorable orientation/organization, so that subsequent intramolecular or intermolecular ligand-based reactions provide the final target molecule.[27–30] Using this strategy, *Sauvage* and coworkers described in the early eighties the successful metal template synthesis of interlocked molecules, in which two aromatic bidentate ligands, held orthogonally by Cu(I), were connected by alkyl chains to give the desired entangled catenates and knots.[27] At the turn of the century, the active metal template approach of a rotaxane was reported, in which a metal ion played both the role of template for linking ligands together and the role of catalyst that allows the intramolecular reactions affecting the complexed ligands.[31] The high coordination numbers (up to 12) found in lanthanide complexes can be taken as an advantage for increasing the ligand density around the central metal and for inducing sophisticated intramolecular reactions between the bound ligands.[6,7] With this in mind, *Gunnlaugsson* and coworkers described the formation of catenanes by using lanthanide-directed synthesis,[7] while *Leigh* and coworkers reported on the use of lanthanide templates for the preparation of chiral molecular knots.[32] In parallel, the lanthanide high coordination number remains a challenge for getting a rational control of *1*) the structural geometry and organization, which result from only minor energy differences[33–35] and *2*) the number of coordinated target ligands and co-ligands that can be completed by solvent molecules and counter-anions.[32,36] Building on this concept, we realized that non-macrocyclic, but highly preorganized multidentate ligands are essentially missing for the efficient capture of neutral [Ln(β-diketonate)$_3$] lanthanide containers, and this despite the attractive magnetic[37,38] and impressive luminescent properties[39–43] of their heteroleptic [**Lk**Ln(β-diketonate)$_3$] adducts. A pioneering attempt aimed at designing the strictly planar and highly delocalized polyaromatic terdentate ligands **L6**,

which were reminiscent of the flexible 2,6-bis-(benzimidazol-2′-yl)pyridine scaffold (*Figure 2,a*).[20] As previously reported for the complexation of **L4** and **L5** with metallic cations,[9,15,19] thorough thermodynamic studies indicated that [**L6**Ln(hfac)$_3$] displayed a preference for the larger metals (*Figure 2,b*), but solid state structures pointed to anomalously long Ln–N$_{bz}$ bonds, which were diagnostic for a very limited fit between the cavity of the planar terdentate ligand **L6** and the entering [Ln(hfac)$_3$] container.[20] As a cure to this drawback, we report here on the unprecedented template synthesis and characterization of the less rigid, yet better preorganized ligand **L7** (*Schemes 1* and *S1*) and its heteroleptic complexes [**L7**Ln(hfac)$_3$], which are compared to their flexible precursors [**1**Ln(hfac)$_3$] and [**L8**Ln(hfac)$_3$] (*Scheme 2*).

Results and Discussion

Synthesis, Characterization and Molecular Structures of Terdentate Ligands **1**, **L7** *and* **L8** *and Their Heteroleptic Adducts [LkLn(hfac)$_3$] (Ln=La, Eu, Gd, Er, Y)*

The target flexible precursor **1** has been synthesized in seven delicate steps from commercial 2,4,6-trimethylpyridine (*Scheme S2*). It is designed for the preparation of a rigid 6-methyl-9,11-dihydro-1*H*,3*H*-2λ^2,10λ^2-pyrido[2,3-*c*:6,5-*c*′]bis(azepine) scaffold decorated with two terminal 5-bromo-1*H*-benzo[*d*]-imidazole as found in **L7**, but the required intramolecular *Grubbs* ring-closing metathesis only failed in our hands (red cross in *Scheme 1*). The crystallographic structure of **1** (*Tables S1*, *S4* and *Figure S123a*) indeed demonstrates a *trans-trans* arrangement of two di-imine units, in which the allyl chains borne by the nitrogen of two benzimidazole side arms are on the opposite side of the vinyl groups bound to the central pyridine ring in order to minimize steric repulsion (*Scheme 2,a*). The same *trans-trans* organization prevails in CD_2Cl_2 as it is evidenced by the lack of Nuclear *Overhauser* Effects (NOE) between the protons of vinyl groups and those of the allyl chains of **1** (*Figure S31*). Altogether, the large distance that separates the reactive double bonds in **1** may explain the failure of intramolecular ring-closing metathesis reactions.

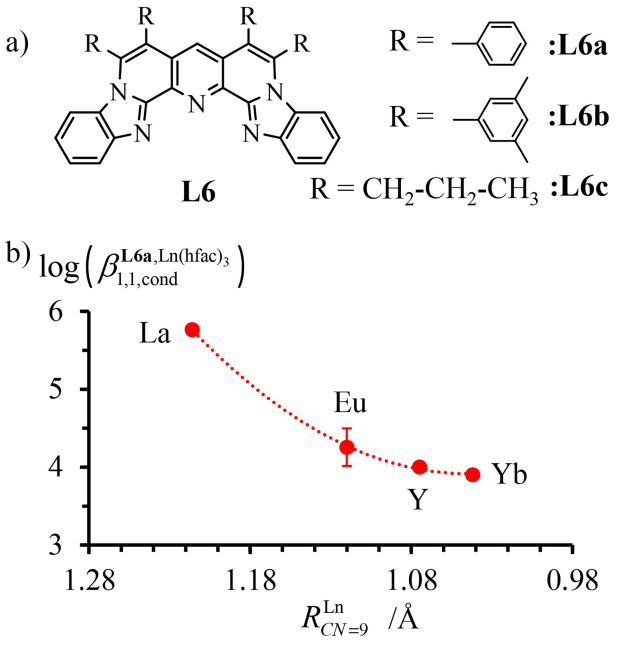

Figure 2. a) Chemical structure of the delocalized aromatic terdentate ligand **L6** and b) associated thermodynamic formation constants of the adduct [**L6**Ln(hfac)$_3$] recorded in dichloromethane + 0.14 M diglyme at 293 K.[20]

In order to overcome this limitation, the complexation of **1** to [(dig)Ln(hfac)$_3$] (Ln=La, Eu, Gd, Y, Er; dig = diglyme) have been considered for forcing the coordinated precursor ligand **1** to accommodate the unfavorable *cis-cis* geometry, which is required for a successful intramolecular metathesis reaction between the terminal olefin groups borne by the pyridine and benzimidazole rings. ^{1}H-NMR titrations of ligand **1** with Ln(hfac)$_3$ containers (Ln=La, Eu, Y) in CD_2Cl_2 at 293 K show the formation of loosely bound heteroleptic [**1**Ln(hfac)$_3$] adducts, which correspond to approximately 70–80% of the total ligand speciation for $|1|_{tot}/|Ln|_{tot} = 1.0$ at millimolar concentrations (*Figures S124–S126*).

The target *trans-trans* to *cis-cis* conformational change of the bis(benzimidazole) scaffold accompanying the complexation of **1** is evidenced by the downfield shift of proton H6, which is located close to the coordinated metal in [**1**Y(hfac)$_3$], while the appearance of the signal of H17 is diagnostic for the presence of the hfac co-ligand bound to the metallic center (*Figure 3a* and *3,b*). Slow diffusion of *tert*-butyl methyl ether into dichloromethane solutions of [**1**Ln-(hfac)$_3$] provided X-ray quality crystals of [**1**Eu(hfac)$_3$] (*Scheme 2a*, *Table S2* and *Figure S123b*) and [**1**Y(hfac)$_3$] (*Table S3*, *Figure S123c*), in which a distorted *cis-cis* conformation of the bound terimine unit can be unambiguously assigned (*Scheme 2a*).

One notes that the benzimidazole-pyridine interplanar angles in the [**1**Ln(hfac)$_3$] adducts are considerable (average $\alpha = 50(2)°$) and reflect the energetic penalty brought by the steric repulsion between the close allyl and vinyl groups. However, the latter

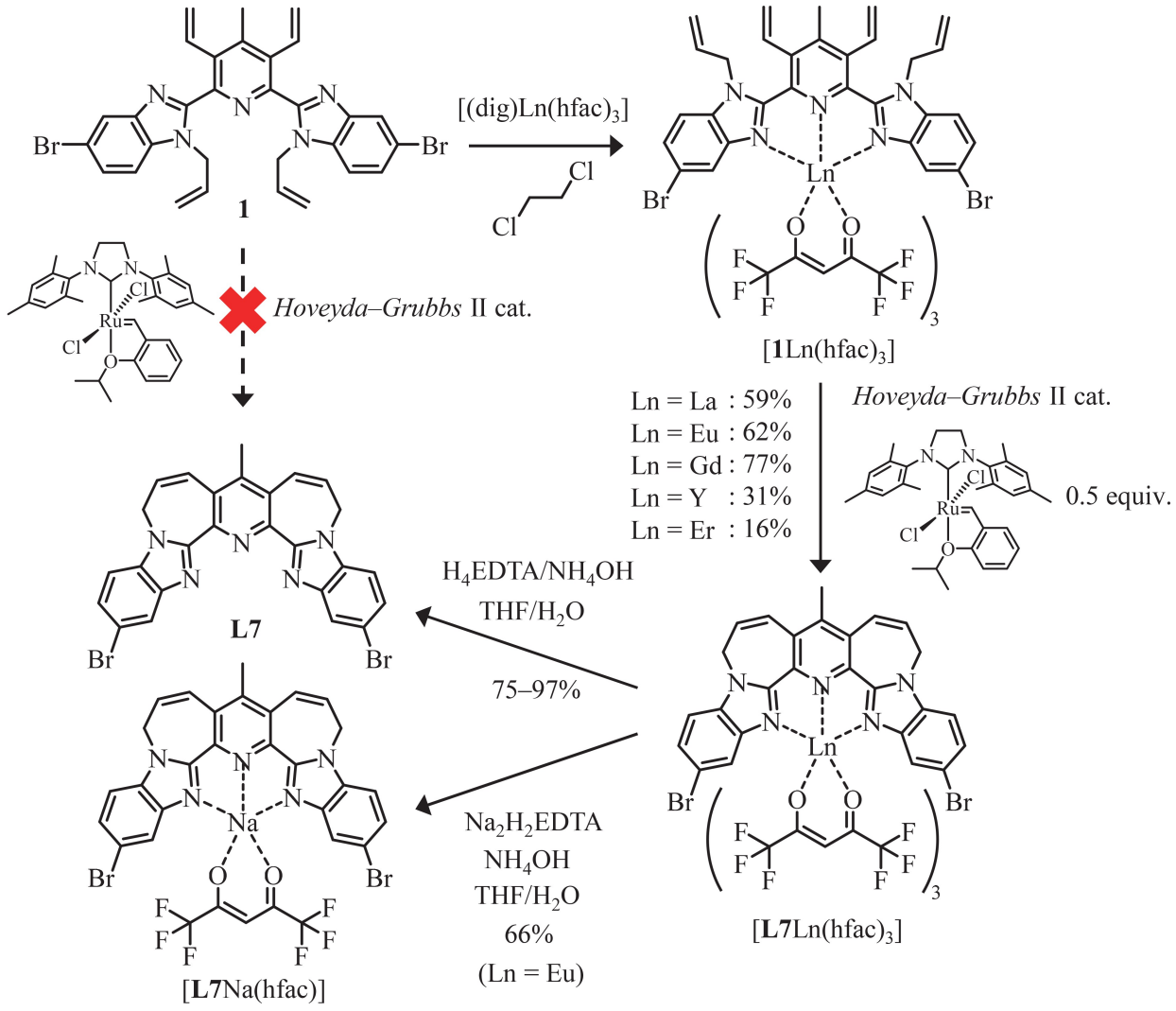

Scheme 1. Synthesis of the terdentate ligand **L7** and its complexes [**L7**Ln(hfac)$_3$] (Ln=La, Eu, Gd, Er, Y).

organization can be exploited as a template effect to perform the target catalyzed ring-closing metathesis reaction (*Scheme 1*). Carrying out the metathesis reaction at low concentrations (0.2 mM) to favor intramolecular cyclization over intermolecular polymerizations[44,45] affords the complexes [**L7**Ln(hfac)$_3$] in limited yields (16–31 %) with small lanthanides (Er, Y), but in good yields (59–77 %) with larger lanthanides (Gd, Eu, La). The lower yields observed with small lanthanides can be accounted for by *1*) some minor decomplexation of the hfac$^-$ anions to give [**L7**Ln(hfac)$_2$]$^+$, as previously established for Ln=Y,[46] that alters the ruthenium-based catalyst[47] and *2*) the difficulties encountered for the separation of the desired neutral compounds [**L7**Ln(hfac)$_3$] from the charged side-products [**L7**Ln(hfac)$_2$]$^+$. The ^{1}H-NMR spectrum of the final complex [**L7**Y(hfac)$_3$] (*Figure 3,c*) shows the disappearance of the signals of the terminal CH_2-alkene groups observed for the [**1**Y(hfac)$_3$] precursor (*Figure 3,b*), together with the detection of new signals, that are characteristic of the formation of newly formed internal double bonds. The vicinal hyperfine coupling constant $J = 10.7$ Hz measured between the two alkene protons H12 and H13 in [**L7**Y(hfac)$_3$] reveals the exclusive formation of a (*Z*)-configuration for the new double bond in agreement with its crystal structure (*Scheme 2,b*). The fact that only the *cis*-isomer is obtained can be assigned to the rigidity of bound **L7**. Upon slow diffusion of *tert*-butyl methyl ether into dichloromethane solutions, single crystals could be obtained for the neutral [**L7**Ln(hfac)$_3$] complexes (Ln=La, Eu,

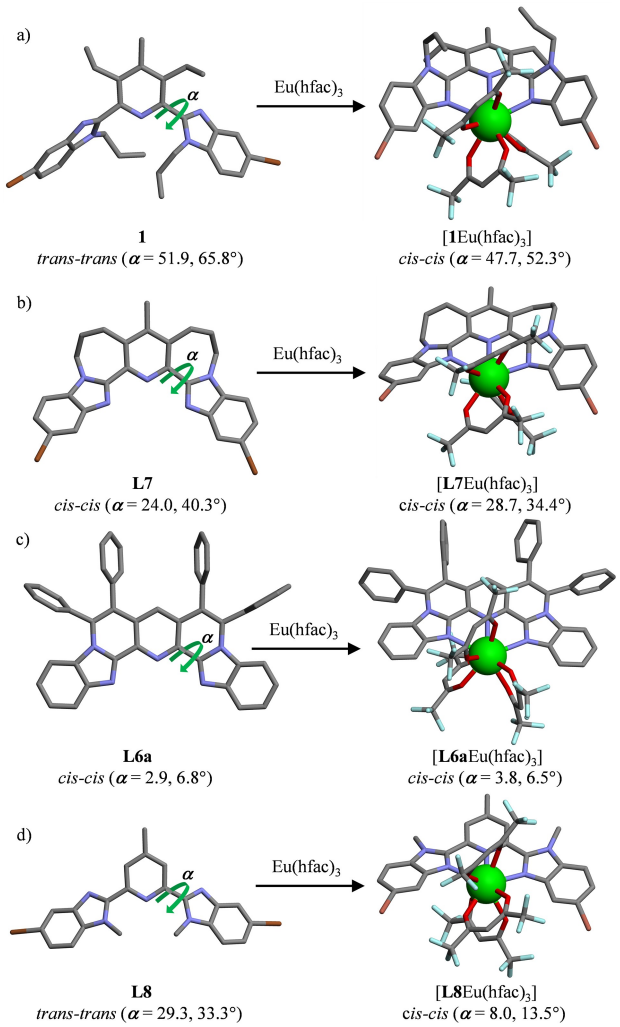

Scheme 2. Molecular structures of a) precursor **1** and its adduct [**1**Eu(hfac)$_3$], b) preorganized ligand **L7** and its adduct [**L7**Eu(hfac)$_3$], c) preorganized ligand **L6a** and its adduct [**L6a**Eu(hfac)$_3$][20] and d) flexible ligand **L8** and its adduct [**L8**Eu(hfac)$_3$] in their crystalline states. Solvent molecules and H-atoms have been omitted for clarity. Color codes: C = grey, N = deep blue, O = red, F = light blue, Br = brown, Eu = green.

Gd, Y, Er; *Tables S10–S24*, *Figure S127*). All molecular structures display similar geometries, in which the central trivalent lanthanide cation is nine-coordinated by three nitrogen atoms of the bound terdentate aromatic ligand **L7** (*cis-cis* conformation) and by six O-atoms of three didentate hfac$^-$ anions (*Scheme 2,b*). Their exact coordination geometries evolve stepwise from muffins for the largest cations (Ln=La, Eu) toward spherical capped square antiprisms for the smaller ones (Ln=Gd, Y, Er, *Table S25*).[47–50]

The Ln–X (X=O, N) bond lengths in [**L7**Ln(hfac)$_3$] complexes display the rough expected stepwise decrease due to the lanthanide contraction along the series (*Tables S26* and *S27*, *Figure S128*).[51–53] Reliable affinities, corrected for the lanthanide contraction, between the N- or O-atoms and the lanthanide center can be computed by using *Eqn. 1*,[54] where v_{ij} is known as the bond valence measuring the affinity of two bound chemical elements *i* and *j*, R_{ij} is the bond valence parameter associated to each specific *i-j* pair,[55–57] d_{ij} is the distance between central atom *i* and donor *j*, and $b = 0.37$ is a universal scaling constant.

$$v_{ij} = e^{\left[\left(R_{ij} - d_{ij}\right)/b\right]} \quad (1)$$

The bond valences computed for Ln–N$_{bz}$ ($\bar{v}_{Ln-N} \approx 0.34$; bz = benzimidazole) and for Ln–O$_{hfac}$ ($\bar{v}_{Ln-O} \approx 0.35$; hfac = hexafluoroacetylacetonate) in the crystals of [**L7**Ln(hfac)$_3$] are comparable and constant along the lanthanide series (*Figure 4,a*). Much smaller values are computed for the central Ln–N$_{py}$ interaction ($0.24 \leq v_{Ln,N} \leq 0.27$; py = pyridine), which regularly increases for the heavier lanthanides (*Figure 4,a* and *Table S28*). This behavior contrasts sharply with the opposite trends reported for the more constrained parent complexes [**L6a**Ln(hfac)$_3$], in which $v_{Ln\text{-}py} \approx v_{Ln\text{-}O} > v_{Ln\text{-}bz,}$ (*Figure 4,c*).[20] In order to set a basic reference for a rational analysis of the role of preorganization in these complexes, we have additionally prepared the model flexible terdentate ligand **L8** (*Scheme 2,d*, *Scheme S3*, *Tables S29–S31* and *Figure S128*). Reaction of **L8** with [(dig)Ln(hfac)$_3$] (Ln=La, Eu, Gd, Er, Y) in dichloromethane generates the complexes [**L8**Ln(hfac)$_3$] in 73–85% yield. Slow diffusion of *tert*-butyl-methylether into dichloromethane solutions provides single crystals for [**L8**La(hfac)$_3$]·CH_2Cl_2, [**L8**Eu(hfac)$_3$]·2($C_5H_{12}O$), [**L8**Gd(hfac)$_3$]·2($C_4H_{10}O$), [**L8**Y(hfac)$_3$]·(CH_2Cl_2) and [**L8**Er(hfac)$_3$·CH_2Cl_2] (*Scheme 2,d*, *Tables S32–S46* and *Figure S129*). The molecular structures of [**L8**Ln(hfac)$_3$] are roughly superimposable with those of [**L7**Ln(hfac)$_3$] for a given lanthanide (*Scheme 2,b* and *2,d*) and their exact coordination geometries evolve from muffins for the largest cation (Ln=La), toward spherical capped square antiprisms for Ln=Eu and, finally, spherical tricapped trigonal prisms for the smaller ones (Ln=Gd, Y, Er, *Table S47*).[47–50] The Ln–N and Ln–O distances are similar in both preorganized [**L7**Ln(hfac)$_3$] (*Tables S26–S27*) and flexible [**L8**Ln(hfac)$_3$] (*Tables S48* and *S49*) complexes and follow the lanthanide contraction along the series. However, a careful look evidences a convex trend for Ln–N bond distances along the lanthanide series for

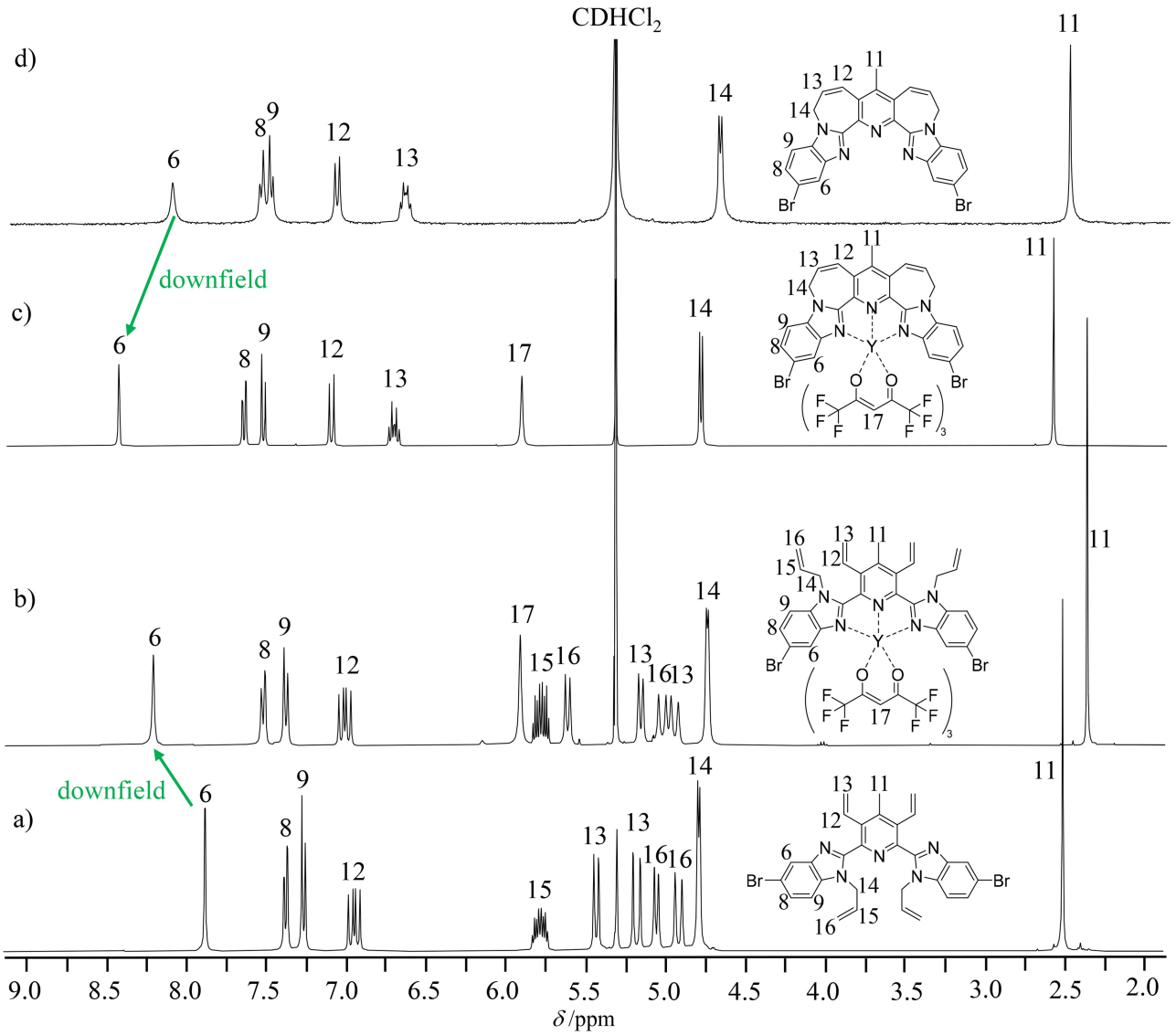

Figure 3. [1]H-NMR spectra of a) precursor **1**, b) complex [**1**Y(hfac)$_3$], c) complex [**L7**Y(hfac)$_3$] and d) ligand **L7** in CD_2Cl_2 solution at 298 K.

flexible complexes [**L8**Ln(hfac)$_3$], while a more linear trend is found for [**L7**Ln(hfac)$_3$] (*Figure S128*). This translates into bowl-shaped bond valences $v_{Ln\text{-}py}$ and $v_{Ln\text{-}bz}$ for [**L8**Ln(hfac)$_3$] along the series (*Figure 4,b* and *Table S50*), which represents the well-established signature[20,58–60] of the binding of flexible 2,6-bis-(benzimidazole-2-yl)pyridine scaffold to Ln(hfac)$_3$. Moreover, $v_{Ln\text{-}bz} > v_{Ln\text{-}py}$ found in [**L8**Ln(hfac)$_3$] mirrors the trend observed for [**L7**Ln(hfac)$_3$]. One can conclude that the rigidification (preorganization) of the bound terdentate ligand in going from **L8** to **L7** has only a minor influence on the Ln–N bond strength in the associated adducts [**Lk**Ln(hfac)$_3$]. The cavities of both ligands in their *cis-cis* conformations are well-suited for catching [Ln(hfac)$_3$] along the lanthanide series. This situation strongly contrasts with the more rigid polyaromatic terdentate **L6a** scaffold, for which the distal Ln–N_{bz} interactions remain unusually weak due to unfavorable sterical constraints (*Scheme 2,c* and *Figure 4,c*).

Finally, the demetallation of [**L7**Ln(hfac)$_3$] with H_4EDTA results in the free ligand **L7** (*Scheme 1*), characterized by an upfield shift of proton H6 and the disappearance of the malonate proton of the $hfac^-$ anion in the [1]H-NMR spectrum of **L7** (*Figure 3,d*). Combined with the NOESY spectrum (*Figure S77*), one can state that ligand **L7** displays *1*) a total number of [1]H-NMR signals pertinent to only one half of aromatic

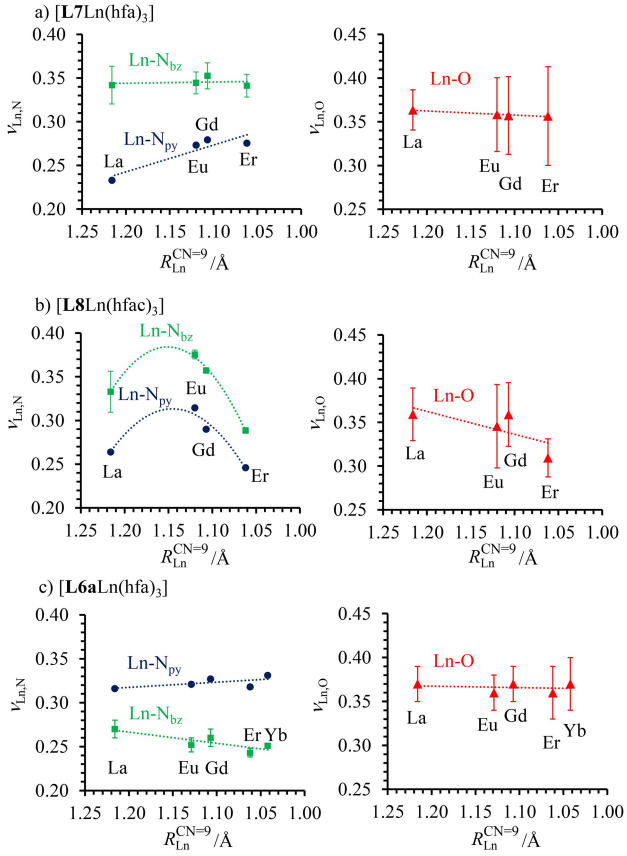

Figure 4. Variation of average Ln–X (X=N, O) bond valences as a function of lanthanide ionic radii in a) [**L7**Ln(hfac)$_3$], b) [**L8**Ln(hfac)$_3$] and c) [**L6a**Ln(hfac)$_3$][20] complexes in their crystalline states. Standard deviations of the averages are shown with vertical error bars. The dashed traces are only guides for the eyes.

protons due to the existence of an average twofold symmetry axis, *2*) enantiotopic methylene protons (H14) due to the existence of an average symmetry plane on the NMR time scale and *3*) a NOE signal between H12 and H11 due to a *cis-cis* arrangement of the diimine units. Altogether, these analyses reveal an average *cis-cis* planar C_{2v} symmetrical arrangement for **L7** in solution that is reminiscent of that found in the crystal structure of **L7**·CH_2Cl_2 (*Scheme 2,b*, *Tables S51–S53* and *Figure S130*). Using Na_2H_2EDTA as a demetallating agent for [**L7**Eu(hfac)$_3$], lead to the unexpected five-coordinate complex [**L7**Na(hfac)] in 66% yield, the structure of which could be confirmed by NMR studies in solution (*Figures S63–S69*) and by single crystal X-ray diffraction in the solid state (*Tables S54–S57* and *Figure S131*).

Thermodynamic Behavior of the Terdentate Ligands (**L7** *and* **L8**) *with Ln(hfac)$_3$ Containers in Dichloromethane (Ln=La, Eu, Y)*

The stability constants of [**Lk**Ln(hfac)$_3$] complexes have been determined by ^{1}H-NMR titrations of **Lk**= **L7**, **L8** with [(dig)Ln(hfac)$_3$] according to *Eqn. 2*. The titrations have been monitored at 293 K in CD_2Cl_2 solution containing an excess of diglyme ([dig]$_{tot}$= 0.14 M) in order to *1*) prevent the fluctuation of the activity coefficients[60] and *2*) reduce the ligand exchange process to the conditional association reaction depicted in *Eqn. 3*. All concentrations are given between vertical lines | | and refer to equilibrium concentrations in this work.

$$[(\mathrm{dig})\mathrm{Ln}(\mathrm{hfac})_3] + \mathbf{Lk} \rightleftharpoons [(\mathbf{Lk})\mathrm{Ln}(\mathrm{hfac})_3] + \mathrm{dig} \qquad \beta^{\mathbf{Lk},\mathrm{Ln}}_{1,1,\mathrm{exch}} \qquad (2)$$

$$[\mathrm{Ln}(\mathrm{hfac})_3] + \mathbf{Lk} \rightleftharpoons [(\mathbf{Lk})\mathrm{Ln}(\mathrm{hfac})_3] \qquad \beta^{\mathbf{Lk},\mathrm{Ln}}_{1,1,\mathrm{cond}} = \frac{\beta^{\mathbf{Lk},\mathrm{Ln}}_{1,1,\mathrm{exch}}}{|\mathrm{dig}|_{tot}} = \frac{|\mathbf{Lk}\mathrm{Ln}(\mathrm{hfac})_3|}{|\mathrm{Ln}(\mathrm{hfac})_3||\mathbf{Lk}|} \qquad (3)$$

Experimentally, the ^{1}H-NMR spectra (*Figure 5* and *Figures S132–S137*) provide reliable integrations for the same proton connected to the free ($I_{\mathbf{Lk}}$) and coordinated ($I_{\mathbf{Lk}\mathrm{Ln}}$) ligand, from which the occupancy factors ($\theta^{\mathrm{Ln}}_{\mathbf{Lk}} = \frac{I_{\mathbf{Lk}\mathrm{Ln}}}{I_{\mathbf{Lk}\mathrm{Ln}}+I_{\mathbf{Lk}}}$) and the free concentrations of the lanthanide containers ($|\mathrm{Ln}|_{\mathrm{free}} = \theta^{\mathrm{Ln}}_{\mathbf{Lk}}|\mathbf{Lk}|_{tot}$) can be calculated with *Eqn. 4* for building the experimental binding isotherms shown in *Figure 6* ($\theta^{\mathrm{Ln}}_{\mathbf{Lk}}$ *versus* log|Ln(hfac)$_3$|, black diamonds).

$$\theta^{\mathrm{Ln}}_{\mathbf{Lk}} = \frac{|\mathrm{Ln}|_{\mathrm{bound}}}{|\mathbf{Lk}|_{tot}} = \frac{|\mathbf{Lk}\mathrm{Ln}(\mathrm{hfac})_3|}{|\mathbf{Lk}|_{tot}} = \frac{I_{\mathbf{Lk}\mathrm{Ln}}}{I_{\mathbf{Lk}\mathrm{Ln}}+I_{\mathbf{Lk}}} = \frac{|\mathrm{Ln}|_{tot}-|\mathrm{Ln}(\mathrm{hfac})_3|}{|\mathbf{Lk}|_{tot}} = \frac{\beta^{\mathbf{Lk},\mathrm{Ln}}_{1,1,\mathrm{cond}}|\mathrm{Ln}(\mathrm{hfac})_3|}{1+\beta^{\mathbf{Lk},\mathrm{Ln}}_{1,1,\mathrm{cond}}|\mathrm{Ln}(\mathrm{hfac})_3|} \qquad (4)$$

Non-linear least-square fits of $\theta^{\mathrm{Ln}}_{\mathbf{Lk}}$ *versus* |Ln(hfac)$_3$| according to the right part of *Eqn. 4*, which considers the exclusive formation of single 1:1 adducts [**Lk**Ln-(hfac)$_3$] during the whole titration process (*Eqn. 3*), give satisfying rebuilt dashed red traces for the titrations of flexible **L8** with [(dig)Ln(hfac)$_3$] along the complete series (Ln=La, Eu, Y; *Figure 6,a*), together with the searched conditional formation constants $\beta^{\mathbf{L8},\mathrm{Ln}}_{1,1,\mathrm{cond}}$ (*Table 1*, *entry 1*).

However, one cannot completely overlook that the fits of $\theta^{\mathrm{Ln}}_{\mathbf{L8}}$ *versus* log(|Ln(hfac)$_3$|) (dashed red

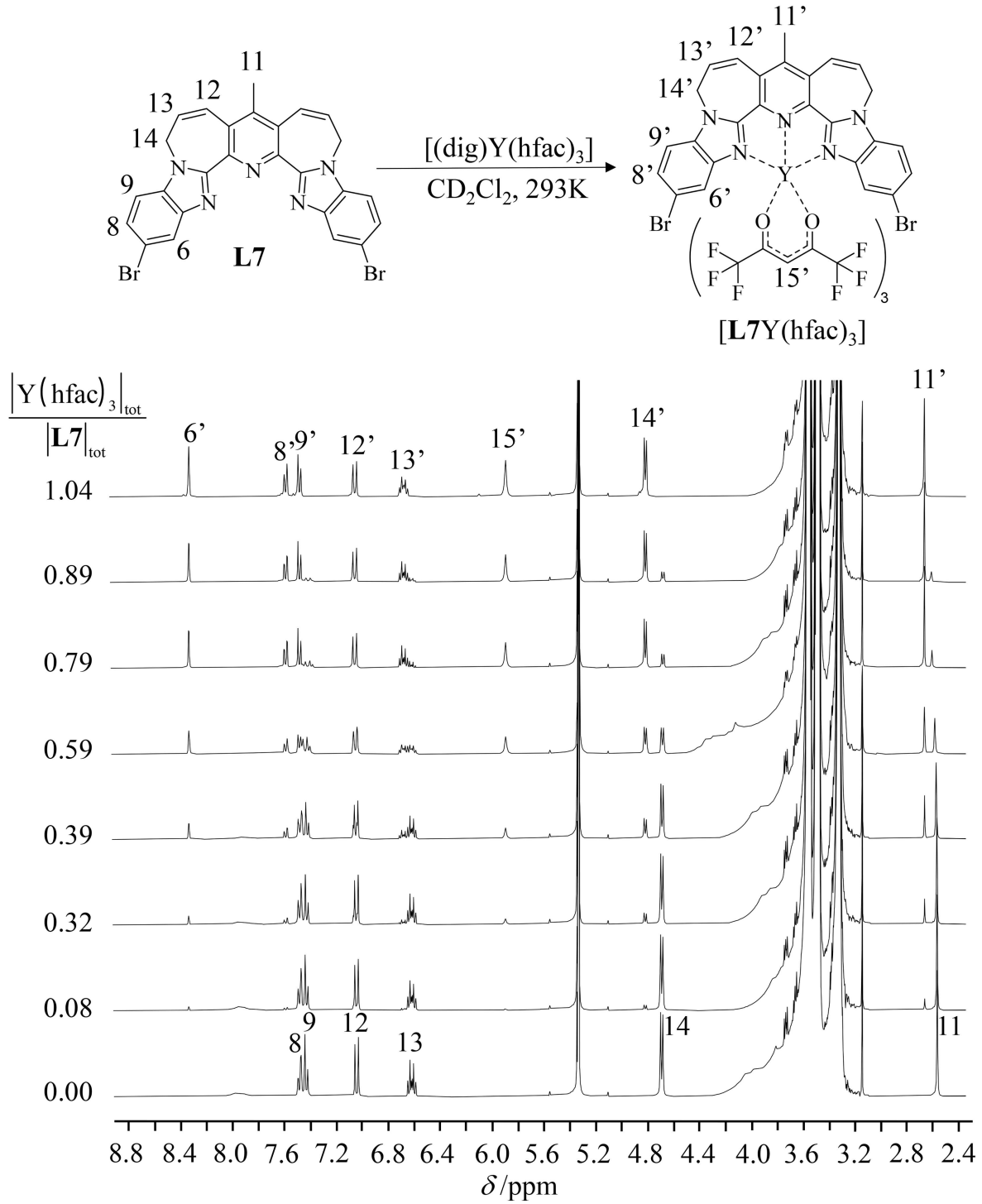

Figure 5. ^{1}H-NMR titration of **L7** (2.51 mm) with [(dig)Y(hfac)$_3$] in CD_2Cl_2 + 0.14 M diglyme at 293 K.

traces in *Figure 6,a*) slightly deviate from the experimental data for Ln = Y (black diamonds in *Figure 6,a*). This behavior can be explained by the changes in activity coefficients γ_i in non-ideal solutions (*Eqn. 5*).[60] Its origin has been assigned to some changes in the solvation energies $\Delta G^{\mathbf{Lk},Ln,S}_{1,1,cond}$ (*Eqn. 6*, $c^{\theta} = 1$ M is the concentration of the reference state), which are not

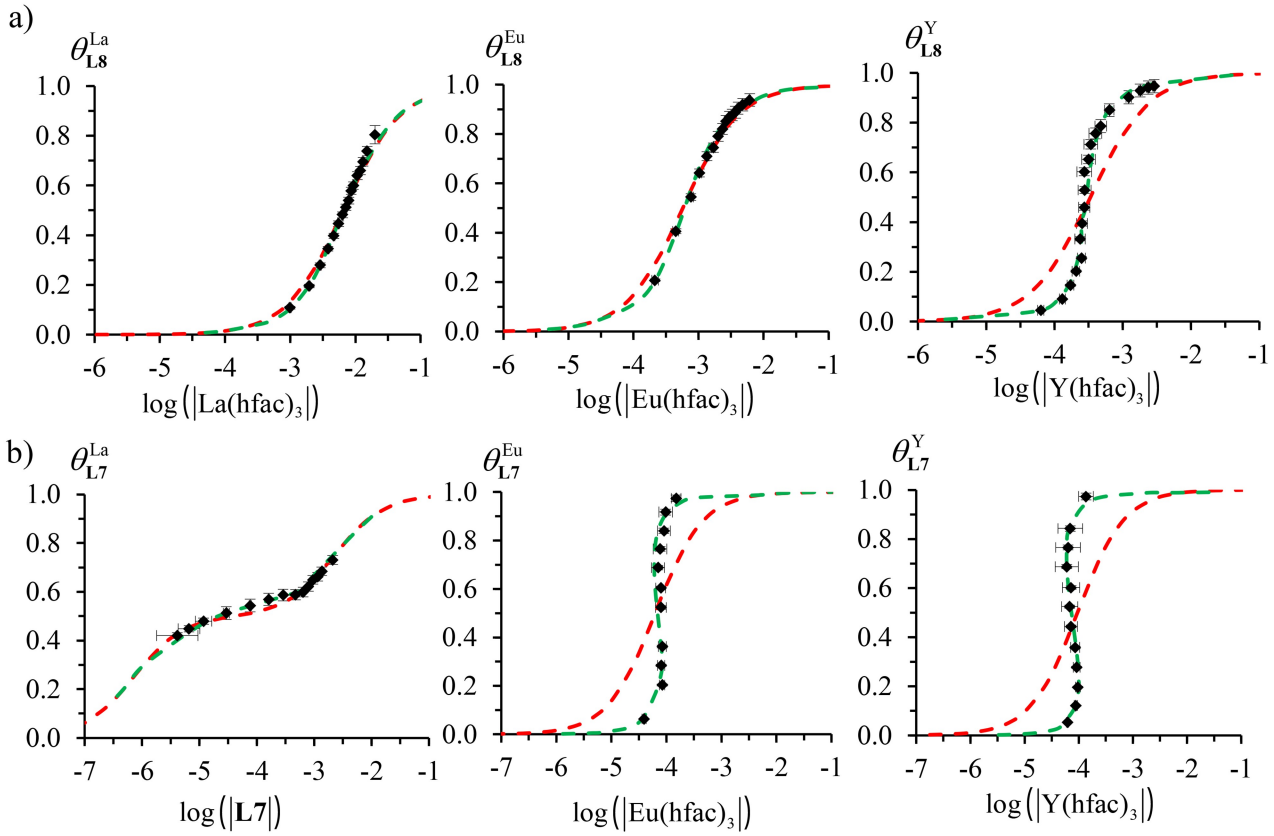

Figure 6. Experimental (black diamonds) and fitted (dashed traces) binding isotherms for the titrations of (a) flexible ligand **L8** and (b) semi-rigid ligand **L7** with [(dig)Ln(hfac)$_3$] in CD_2Cl_2 + 0.14 M diglyme at 293 K. The dashed red traces are obtained by using *Eqn. 4* and $\beta^{\mathbf{Lk},Ln}_{1,1,cond}$ taken from *Table 1* (*entry 1*). The dashed green traces are obtained by using *Eqn. 7* and $\Delta G^{\mathbf{Lk},Ln,\infty}_{1,1,cond}$ and $\Delta G^{\mathbf{Lk},Ln,S}_{1,1,cond}$ taken from *Table 1* (*entries 7* and *8*). For [(**L7**)$_m$La(hfac)$_3$], *Eqn. 9* applies with $\beta^{L7,La}_{1,1,cond}$ and $\beta^{L8,La}_{2,1,cond}$ taken from *Table 2* (*entries 1* and *2*) to give the dashed red trace, while *Eqns. A3–7* and *A3–8* developed in *Appendix 1* (*Supporting Information*) are used for computing the dashed green trace.

considered in the standard states of the pure reactants and products.[61,62]

$$\beta^{\mathbf{Lk},Ln}_{1,1,cond} = \frac{a^{eq}_{\mathbf{Lk}Ln}}{a^{eq}_{Ln}a^{eq}_{\mathbf{Lk}}} = \frac{\gamma_{\mathbf{Lk}Ln}}{\gamma_{Ln}\gamma_{\mathbf{Lk}}}\cdot\frac{(c^{eq}_{\mathbf{Lk}Ln}/c^{\theta})}{(c^{eq}_{Ln}/c^{\theta})(c^{eq}_{\mathbf{Lk}}/c^{\theta})} = \frac{\gamma_{\mathbf{Lk}Ln}}{\gamma_{Ln}\gamma_{\mathbf{Lk}}}\cdot\left(\frac{|\mathbf{Lk}Ln(hfac)_3|}{|Ln(hfac)_3||\mathbf{Lk}|}\right)\cdot c^{\theta} = \frac{\gamma_{\mathbf{Lk}Ln}}{\gamma_{Ln}\gamma_{\mathbf{Lk}}}\cdot Q^{\mathbf{Lk},Ln}_{1,1,cond}\cdot c^{\theta} \quad (5)$$

$$-RT\ln\left(Q^{\mathbf{Lk},Ln}_{1,1,cond}\right) = -RT\ln\left(\beta^{\mathbf{Lk},Ln,\infty}_{1,1,cond}\right) + \Delta G^{\mathbf{Lk},Ln,S}_{1,1,cond}\cdot\left(|\mathbf{Lk}Ln(hfac)_3|/c^{\theta}\right) \quad (6)$$

The theoretical reconciliation between the experimental quotients of reaction $Q^{\mathbf{Lk},Ln}_{1,1,cond}$ and the thermodynamic stability constant at infinite dilution $\beta^{\mathbf{Lk},Ln,\infty}_{1,1,cond}$ is given in *Eqn. 6* and experimentally confirmed by the satisfying linear dependences of $-RT\ln\left(Q^{\mathbf{Lk},Ln}_{1,1,cond}\right)$ with respect to the advance of the complexation reaction measured by the increasing concentrations of the formed complexes $|\mathbf{Lk}Ln(hfac)_3|$ (*Figure 7*).

The resulting free energy changes at infinite dilution $\Delta G^{Ln,\mathbf{Lk},\infty}_{1,1,cond} = -RT\ln\left(\beta^{Ln,\mathbf{Lk},\infty}_{1,1,cond}\right)$ and the 'solvation correction' $\Delta G^{Ln,\mathbf{Lk},S}_{1,1,cond}$ are collected in *Table 1* (*entries 7* and *8*). Finally, the improved rebuilt occupancy factor $\theta^{Ln}_{\mathbf{Lk}}$ computed for each $\langle|\mathbf{Lk}|_{tot};|Ln|_{tot}\rangle$ pair is obtained by solving *Eqn. 7* for $|Ln(hfac)_3|$, which eventually provides the binding isotherms shown as green dashed traces in *Figure 6,a.*[20]

Table 1. Thermodynamic conditional stability constants $\beta^{\mathbf{Lk},\mathrm{Ln}}_{1,1,\mathrm{cond}}$ (*Eqn. 3*) and $\beta^{\mathbf{Lk},\mathrm{Ln}}_{2,1,\mathrm{cond}}$ (*Eqn. 8*), intrinsic affinities $f^{\mathbf{Lk},\mathrm{Ln}}_{\mathrm{asso,cond}}$ (*Eqn. 11*), interligand interactions $u^{\mathbf{Lk}-\mathbf{Lk}}_{\mathrm{cond}} = exp\left(-\Delta E^{\mathbf{Lk}-\mathbf{Lk}}_{\mathrm{cond}}/RT\right)$ (*Eqn. 12*) and thermodynamic free energies $\Delta G^{\mathbf{Lk},\mathrm{Ln}}_{n,1,\mathrm{cond}} = -RT\ln\left(\beta^{\mathbf{Lk},\mathrm{Ln}}_{n,1,\mathrm{cond}}\right)$, $\Delta G^{\mathbf{Lk},\mathrm{Ln},\infty}_{1,1,\mathrm{cond}}$ and $\Delta G^{\mathbf{Lk},\mathrm{Ln},\mathrm{S}}_{1,1,\mathrm{cond}}$ determined for the titrations of **L7** and **L8** with [(dig)Ln(hfac)$_3$] (Ln = La, Eu, Y) in CD_2Cl_2 + 0.14 M diglyme at 293 K.

	Ln	**L8**	**L7**
$\beta^{\mathbf{Lk},\mathrm{Ln}}_{1,1,\mathrm{cond}}$	La	153(8)	$1.4(1)\cdot10^{6}$
	Eu	$1.7(1)\cdot10^{3}$	$1.6(6)\cdot10^{4}$
	Y	$3.1(1)\cdot10^{3}$	$1.1(6)\cdot10^{4}$
$\beta^{\mathbf{Lk},\mathrm{Ln}}_{2,1,\mathrm{cond}}$	La	0	$6.2(2)\cdot10^{8}$
$f^{\mathbf{Lk},\mathrm{Ln}}_{\mathrm{asso,cond}}$	La	76(4)	$7.0(5)\cdot10^{5}$
	Eu	$8.5(1)\cdot10^{2}$	$8.0(3)\cdot10^{3}$
	Y	$1.6(1)\cdot10^{3}$	$5.5(3)\cdot10^{3}$
$u^{\mathbf{Lk}-\mathbf{Lk}}_{\mathrm{cond}}$	La	0	$3.2(3)\cdot10^{-4}$
$\Delta G^{\mathbf{Lk},\mathrm{Ln}}_{1,1,\mathrm{cond}}$/kJ·mol^{-1}	La	−12.3(1)	−34.5(3)
	Eu	−18.2(1)	−23.6(4)
	Y	−19.6(1)	−22.6(5)
$\Delta G^{\mathbf{Lk},\mathrm{Ln}}_{2,1,\mathrm{cond}}$/kJ·mol^{-1}	La	0	−49.3(3)
$\Delta G^{\mathbf{Lk},\mathrm{Ln},\infty}_{1,1,\mathrm{cond}}$/kJ·mol^{-1}	La	−11.4(1)	−19.4(1.0)[a]
	Eu	−16.7(3)	−16.7(5)
	Y	−17.4(8)	−16.1(1)
$\Delta G^{\mathbf{Lk},\mathrm{Ln},\mathrm{S}}_{1,1,\mathrm{cond}}$/kJ·mol^{-1}	La	−979(103)	$-7.8(7)\cdot10^{3}$[a]
	Eu	$-1.5(3)\cdot10^{3}$	$-5.7(3)\cdot10^{3}$
	Y	$-2.2(6)\cdot10^{3}$	$-6.1(1)\cdot10^{3}$

[a] Calculation is detailed in *Appendix 1* (*Supporting Information*).

$$\theta^{\mathrm{Ln}}_{\mathbf{Lk}} = \frac{Q^{\mathrm{Ln},\mathbf{Lk}}_{1,1,\mathrm{cond}}|\mathrm{Ln(hfac)_3}|}{1+Q^{\mathrm{Ln},\mathbf{Lk}}_{1,1,\mathrm{cond}}|\mathrm{Ln(hfac)_3}|} = \frac{|\mathbf{Lk}\mathrm{Ln(hfac)_3}|}{|\mathbf{Lk}|_{\mathrm{tot}}} = \frac{|\mathrm{Ln}|_{\mathrm{tot}} - |\mathrm{Ln(hfac)_3}|}{|\mathbf{Lk}|_{\mathrm{tot}}} =$$

$$\frac{|\mathrm{Ln(hfac)_3}|}{1+\left\{\exp\left[-\left(\begin{array}{l}\Delta G^{\mathrm{Ln},\mathbf{Lk},\infty}_{1,1,\mathrm{cond}} + (|\mathrm{Ln}|_{\mathrm{tot}} - |\mathrm{Ln(hfac)_3}|)\cdot \\ \\ \Delta G^{\mathrm{Ln},\mathbf{Lk},\mathrm{S}}_{1,1,\mathrm{cond}}\end{array}\right)/RT\right]\cdot \right.} \quad (7)$$
$$\left. |\mathrm{Ln(hfac)_3}| \right\}$$

The same approach holds for titrations of preorganized **L7** with [(dig)Ln(hfac)$_3$] in CD_2Cl_2 + 0.14 M diglyme (*Figures 6,b* and *7,b*). Larger stability constants $\beta^{\mathbf{L7},\mathrm{Ln}}_{1,1,\mathrm{cond}}$ (*Table 1*, *entry 1*, and *Figure 8*) are observed together with the detection of minor amounts of the di-adduct [(**L7**)$_2$La(hfac)$_3$] with the largest lanthanum metal (*Figure S133*). This behavior is reminiscent to that previously reported for closely analogous terdentate complexes, for which the molecular structure of a ten-coordinated *pseudo*-bicapped square-antiprismatic double-stranded $[(\mathbf{Lk})_2\mathrm{La(hfac)_2}]^+$ adduct could be observed in the crystal structure of the [(**Lk**)$_2$La-(hfac)$_2$]$_2$[La$_2$(hfac)$_4$(O$_2$CCF$_3$)$_4$] salt.[46] In this situation, *Eqn. 3* must be completed with *Eqn. 8*, and the binding isotherm in *Eqn. 9* now considers [La(hfac)$_3$] as the host to which two **L7** guest molecules can be successively bound. The non-linear least square fits of the experimental data (black diamonds in *Figure 6,b* for Ln = La) with the help of *Eqn. 9* provides the two cumulative stability constants $\beta^{\mathbf{L7},\mathrm{La}}_{1,1,\mathrm{cond}}$ and $\beta^{\mathbf{L7},\mathrm{La}}_{2,1,\mathrm{cond}}$ gathered in *Table 1* (*entries 1* and *2*). The rebuilt binding isotherm is shown as a dashed red trace in *Figure 6,b* (left).

$$[\mathrm{Ln(hfac)_3}] + 2\mathbf{Lk} \;\; [(\mathbf{Lk})_2\mathrm{Ln(hfac)_3}]$$
$$\beta^{\mathbf{Lk},\mathrm{Ln}}_{2,1,\mathrm{cond}} = \frac{\beta^{\mathbf{Lk},\mathrm{Ln}}_{2,1,\mathrm{exch}}}{|\mathbf{dig}|_{\mathrm{tot}}} = \frac{|(\mathbf{Lk})_2\mathrm{Ln(hfac)_3}|}{|\mathrm{Ln(hfac)_3}||\mathbf{Lk}|^2} \quad (8)$$

$$\theta^{\mathbf{Lk}}_{\mathrm{La}} = \frac{|\mathbf{Lk}|_{\mathrm{bound}}}{2|\mathrm{La}|_{\mathrm{tot}}} = \frac{|\mathbf{Lk}|_{\mathrm{tot}}}{2|\mathrm{La}|_{\mathrm{tot}}}\left(\frac{I_{\mathbf{Lk}\mathrm{La}} + I_{\mathbf{Lk}_2\mathrm{La}}}{I_{\mathbf{Lk}} + I_{\mathbf{Lk}\mathrm{La}} + I_{\mathbf{Lk}_2\mathrm{La}}}\right) =$$
$$\frac{|\mathbf{Lk}|_{\mathrm{tot}} - |\mathbf{Lk}|}{2|\mathrm{La}|_{\mathrm{tot}}} = \frac{\beta^{\mathbf{Lk},\mathrm{Ln}}_{1,1,\mathrm{cond}}|\mathbf{Lk}| + 2\beta^{\mathbf{Lk},\mathrm{Ln}}_{2,1,\mathrm{cond}}|\mathbf{Lk}|^2}{2\left(1+\beta^{\mathbf{Lk},\mathrm{Ln}}_{1,1,\mathrm{cond}}|\mathbf{Lk}| + \beta^{\mathbf{Lk},\mathrm{Ln}}_{2,1,\mathrm{cond}}|\mathbf{Lk}|^2\right)} \quad (9)$$

The application of *Eggers'* model (reminiscent to *Eqn. 6*)[59–62] to fit the binding isotherm for the 1:2 complex ([(**L7**)$_2$La(hfac)$_3$]) using variable activity coefficients is detailed in *Appendix 1*. It did not improve significantly the fit as exemplified by the green dashed trace built in *Figure 6,b*, left.

At millimolar concentrations in dichloromethane, the conditional association constants $\beta^{\mathbf{Lk},\mathrm{Ln}}_{1,1,\mathrm{cond}}$ for the formation of the [**Lk**Ln(hfac)$_3$] adducts with the two flexible ligands **L8** (orange squares in *Figure 8* and *Figure S138a*) and **L9** (blue squares)[20] confirm the decrease in affinity by a factor 2 when Br-atoms are connected to the 5-position of the peripheral benzimidazole side arms.[63] Despite this unfavorable inductive effect, the novel di-bromo substituted preorganized ligand **L7** produces [**L7**Ln(hfac)$_3$] adducts (green disks in *Figure 8* and *Figure S138a*) which are more stable than their counterparts with the non-substituted rigid **L6a** analogue (red disks). For both

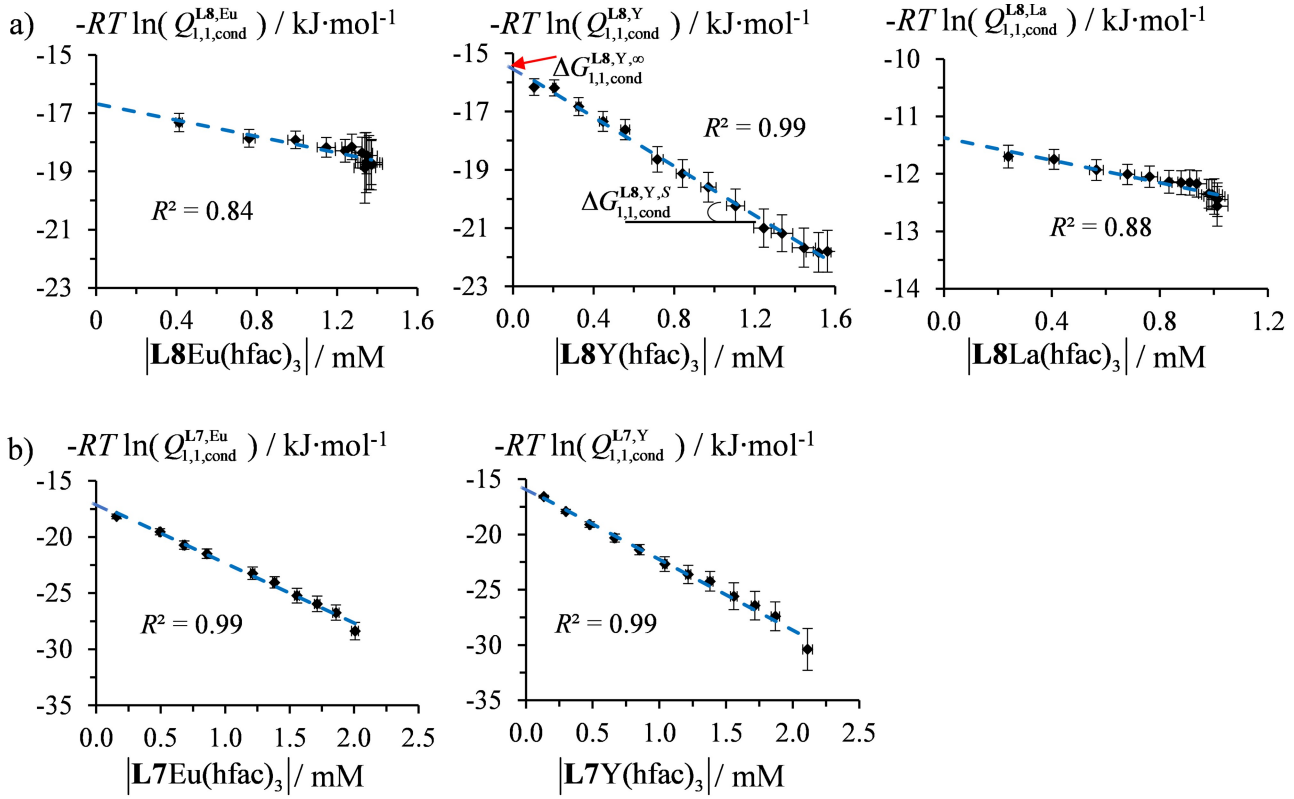

Figure 7. Plots of $-RT\ln(Q^{Lk,Ln}_{1,1,cond})$ as a function of $|Lk\mathrm{Ln(hfac)_3}|$ for the titrations of a) **L8**, and b) **L7**, with [(dig)Ln(hfac)$_3$] in CD_2Cl_2 + 0.14 M diglyme at 293 K (experimental = black diamonds and linear least-square fits = dashed blue traces). According to *Eqn. 6*, $\Delta G^{Lk,Ln,\infty}_{1,1,cond}$ corresponds to the ordinate and $\Delta G^{Lk,Ln,S}_{1,1,cond}$ to the slope of the linear traces.

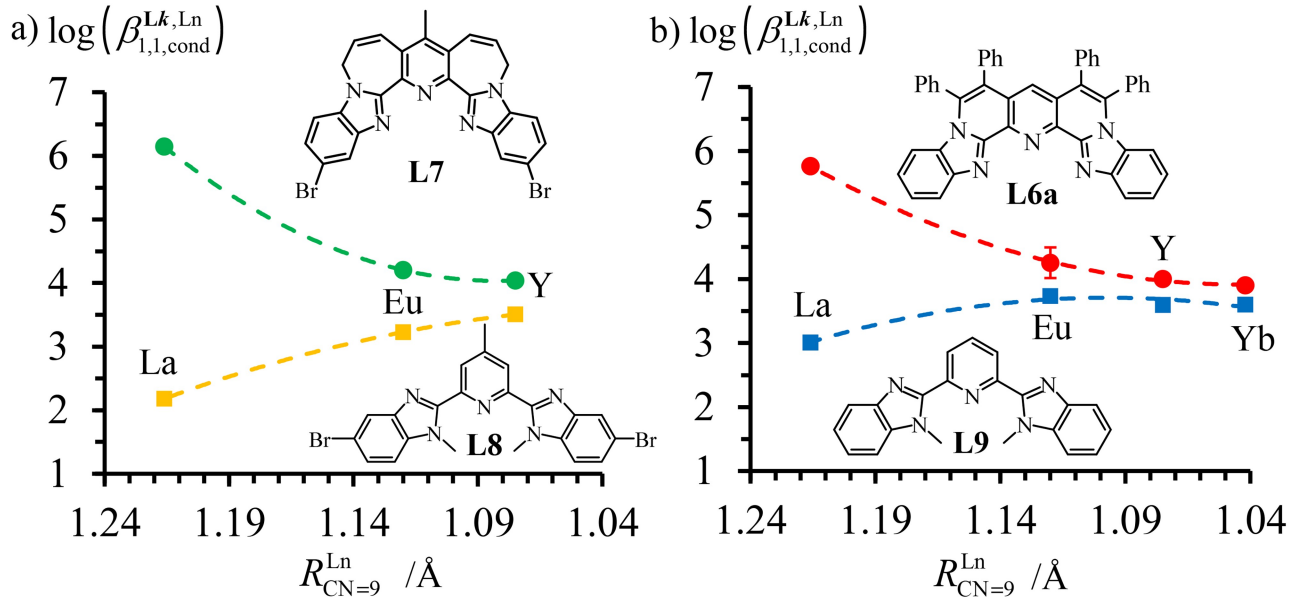

Figure 8. Conditional thermodynamic association constants for the formation of 1:1 complexes [**Lk**Ln(hfac)$_3$] in CD_2Cl_2 + 0.14 M diglyme for a) ligands **L7** and **L8** and b) ligands **L6a** and its flexible precursor **L9**.[20] The dashed traces are only guides for the eyes.

preorganized ligands **L7** and **L6a**, an anti-electrostatic selectivity is detected along the lanthanide series (La > Eu ≈ Y), whereas the parent flexible ligands **L8** and **L9** exhibit the opposite trend. Extrapolation at infinite dilution highlights significant drifts due to the variation of the activity coefficients as caught by *Eggers'* model (*Eqn. 6* and *Table 1*, *entries 7* and *8*), but the thermodynamic gain of replacing flexible (**L8** or **L9**) with their preorganized counterparts (**L7** and **L6a**) remains a fully valid concept (*Figure S138b*).

Finally, following *Benson*'s approach,[64] the conditional formation constants $\beta_{n,1,\mathrm{cond}}^{\mathbf{Lk},\mathrm{Ln}}$ can be separated into two contributions in *Eqn. 10*. Firstly, a statistical factor $\omega_{n,1}^{\mathbf{Lk},\mathrm{Ln}}$ that takes into account the pure statistical contribution due to the change in the molecular rotational entropies when the reactants are transformed into products.[65,66] It can be easily computed by using the symmetry number technique detailed in *Appendix 2*. Secondly, a chemical part $K_{n,1,\mathrm{chem}}^{\mathbf{Lk},\mathrm{Ln}}$, which measures the associated change in energies accompanying the reorganization of the multi-components interactions (including solvation effects).[67]

$$\beta_{n,1,\mathrm{cond}}^{\mathbf{Lk},\mathrm{Ln}} = \omega_{n,1}^{\mathbf{Lk},\mathrm{Ln}} K_{n,1,\mathrm{chem}}^{\mathbf{Lk},\mathrm{Ln}} \tag{10}$$

The chemical part $K_{n,1,\mathrm{chem}}^{\mathbf{Lk},\mathrm{Ln}}$ can be further dissected into inter-component $f_{\mathrm{asso,cond}}^{\mathbf{Lk},\mathrm{Ln}}$ (*Table 1*, *entry 3* with $\Delta G_{\mathrm{asso,inter}}^{\mathrm{Ln},\mathbf{Lk},} = -RT\ln\left(f_{\mathrm{asso,cond}}^{\mathbf{Lk},\mathrm{Ln},}\right)$) and intra-component $u_{\mathrm{cond}}^{\mathbf{Lk},\mathbf{Lk}}$ (*Table 1*, *entry 4* with $\Delta E_{\mathrm{inter}}^{\mathbf{Lk},\mathbf{Lk},} = -RT\ln\left(u_{\mathrm{cond}}^{\mathbf{Lk},\mathbf{Lk}}\right)$) contributions with the help of the site-binding model (*Eqns. 11* and *12*).[20,67]

$$\beta_{1,1,\mathrm{cond}}^{\mathbf{Lk},\mathrm{Ln}} = \omega_{1,1}^{\mathbf{Lk},\mathrm{Ln}} f_{\mathrm{asso,cond}}^{\mathbf{Lk},\mathrm{Ln}} = 2 f_{\mathrm{asso,cond}}^{\mathbf{Lk},\mathrm{Ln}} \tag{11}$$

$$\beta_{2,1,\mathrm{cond}}^{\mathbf{Lk},\mathrm{Ln}} = \omega_{2,1}^{\mathbf{Lk},\mathrm{Ln}} \left(f_{\mathrm{asso,cond}}^{\mathbf{Lk},\mathrm{Ln}}\right)^2 u_{\mathrm{cond}}^{\mathbf{Lk},\mathbf{Lk}} = 4\left(f_{\mathrm{asso,cond}}^{\mathbf{Lk},\mathrm{Ln}}\right)^2 u_{\mathrm{cond}}^{\mathbf{Lk},\mathbf{Lk}} \tag{12}$$

Obviously, the computed conditional inter-component associations $f_{\mathrm{asso,cond}}^{\mathbf{Lk},\mathrm{Ln}}$ between **Lk** and [Ln(hfac)$_3$] strictly mirror the thermodynamic trends established for $\beta_{1,1,\mathrm{cond}}^{\mathbf{Lk},\mathrm{Ln}}$ (*Eqn. 11* and *Figure 8*). Interestingly, *Eqn. 12* provides an estimate of $\Delta E_{\mathrm{cond}}^{\mathbf{L7}-\mathbf{L7},} = -RT\ln\left(u_{\mathrm{cond}}^{\mathbf{L7}-\mathbf{L7}}\right) =$ 19.6 kJ mol^{-1} for the considerable anti-cooperative process accompanying the successive binding of two ligands **L7** to [La(hfac)$_3$].

Altogether, the affinities of the preorganized ligand **L7** for [Ln(hfac)$_3$] cations are larger by factors 3 to 9000 than those of the flexible ligand **L8** for the same lanthanide containers (*Table 1*, *entry 3*). This phenomenon can be assigned to the energy penalty produced by the rotation of the benzimidazole side arms, which is required for the binding of **L8** to the lanthanide metal but is absent with the preorganized ligand **L7**. Compared with the closely related ligand pairs **L9** (flexible)/**L6a** (preorganized),[20] the gain in stability upon preorganization is larger by at least one order of magnitude in going from **L8** to **L7**, which compensates for the detrimental connection of electro-attractive Br-atoms. This makes **L7** eligible for its incorporation into linear polymeric scaffolds.[63] We also note that *1*) both preorganized terdentate ligands **L6a** and **L7** exhibit a pronounced preference for the large lanthanide metals (*Figure 8*), and *2*) no dissociation of hfac$^-$ co-ligand can be detected at millimolar concentration in dichloromethane for all complexes except for [**L8**Y(hfac)$_3$], the ^{1}H-NMR spectrum of which evidenced some traces of [**L8**Y(hfac)$_2$]$^+$ and hfac$^-$ (*Figure S139*).

Finally, the absorption spectra recorded in dichloromethane solution show remarkable complementarities for the two preorganized ligands **L7** and **L6a** (*Figure 9,a*), and for their [**Lk**Ln(hfac)$_3$] adducts (*Figure 9,b*). The highly delocalized 30π-electron aromatic structure of **L6a** (red traces in *Figure 9*) possesses low-energy electronic states reaching the visible part (400–450 nm) of the electromagnetic domain. This makes this ligand attractive for the visible sensitization of lanthanide-based NIR emitters (Ln=Nd, Er, Yb), but it restricts linear light-upconversion to final excited states emitting at wavelengths longer than 500 nm. The introduction of two additional methylene units into the pyridine-benzimidazole bridges in **L7** breaks aromatic electronic delocalization and no ligand-centered absorption band can be detected at wavelengths longer than 360 nm (green traces in *Figure 9*).

Conclusion

The synthesis of the preorganized terdentate ligand **L7** exploits a *Grubbs* ring-closing metathesis between terminal olefin groups, which appeared to be only possible when the later groups are held close together by a template reaction using a neutral [Ln(β-diketonate)$_3$] lanthanide container. During the template complexation process, only one molecule of the ligand precursor **1** is connected to the trivalent lanthanide ion thanks to a strict control of the coordination number via the complementary binding of three anionic bidentate hfac$^-$ co-ligands. Large lanthanides (Ln=La, Eu, Gd) better match the sterical constraints required for the formation of the final 1,2,3,9,10,11-hexahydropyrido[2,3-*c*:6,5-*c*']bis(azepine)

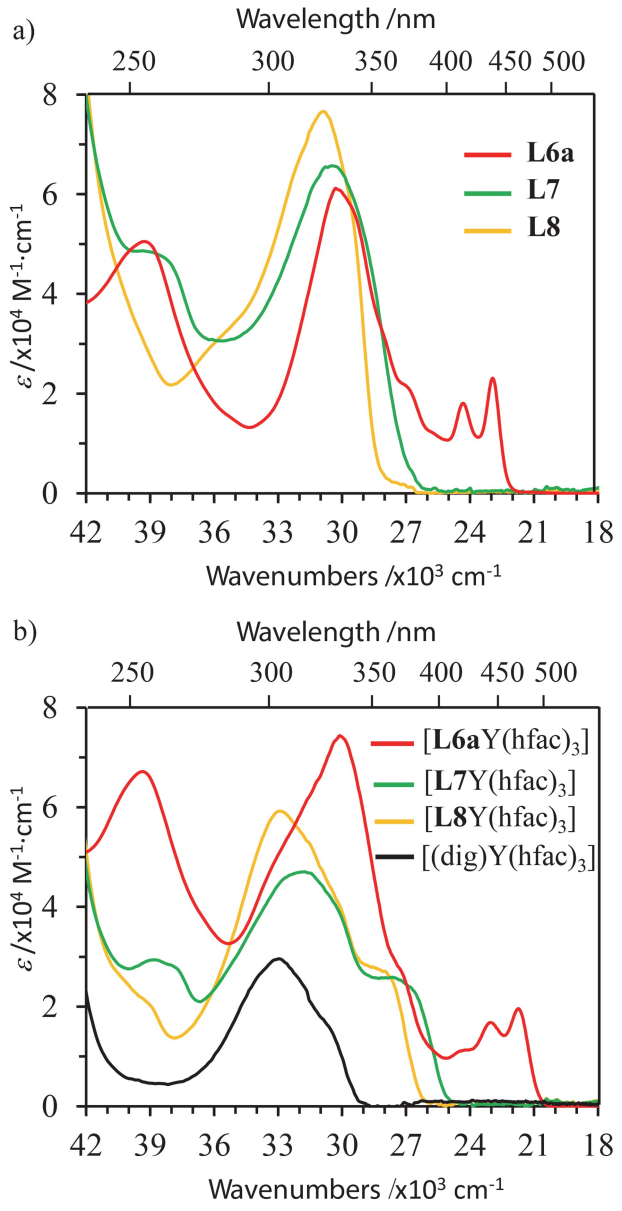

Figure 9. Absorption spectra of a) ligands **L7**, **L8** and **L6a**[20] and b) complexes [**Lk**Y(hfac)$_3$] in CH_2Cl_2 solution (10^{-5} M, 293 K). The computed dissociation of the [**Lk**Y(hfac)$_3$] adducts does not exceed 4% in these conditions.

scaffold in good yields. The crystal structures of the [**L7**Ln(hfac)$_3$] adducts show that the two seven-membered 2,7-dihydro-1*H*-azepine rings, which connect the central pyridine rings to the benzimidazole side arms in **L7** (*Scheme 2,b*), favorably preorganize the peripheral N_{bz} donor atom for their efficient binding to [Ln(hfac)$_3$] (*Figure 4,a*). The opposite, and unfavorable situation held with the previously reported rigid ligand **L6a**,[20] because the shorter six-membered 1,2-dihydropyridine bridging rings (*Scheme 2,c*) prevented the effective connection of the peripheral benzimidazole ring to the lanthanide cation in [**L6a**Ln(hfac)$_3$] (*Figure 4,c*).

Thermodynamic studies in dichloromethane confirm *1*) the optimum fit between the cavity of **L7** and large lanthanide cations and *2*) the considerable benefit of preorganizing the ligand strand in going from flexible **L8** to rigid **L7**. Compared with its **L6a** analogue, the stabilities of [**L7**Ln(hfac)$_3$] are systematically larger (*Figure 8*), and this is despite the connection of two terminal unfavorable electron-withdrawing Br-atoms, which are required for the further introduction of this terdentate unit into linear oligomers and polymers. On the other hand, the selectivity of ligand **L8** for heavy lanthanides contrasts with the reverse trend evidenced with the preorganized ligand **L7**. These characteristics could be exploited *1*) for designing heterometallic lanthanidopolymers with controlled intermetallic communications and associated photophysical properties[68–70] and *2*) for separating lanthanide ions by selective complexation reactions.[71–73]

Finally, whereas light-downshifting processes are probably more attractive with [**L6a**Ln(hfac)$_3$], the design of a 'broken' polyaromatic structure in [**L7**Ln(hfac)$_3$] clears the visible part of the electromagnetic spectrum from ligand-centered excited states and paves the way for exploiting in a forthcoming contribution this ligand for Er-based linear molecular upconversion implemented in soluble polymers.[74]

Experimental Section

General

All reagents were purchased from *Alfa Aesar*, *FluoroChem*, *Acros*, *Fischer Chemicals AG* and *Sigma-Aldrich*, and used as received. NMR Spectra were recorded on a *Bruker Avance* 400 MHz spectrometers. The experiments were recorded at 25 °C and the solvent was used as an internal reference. Pneumatically assisted electrospray (ESI) mass spectra were recorded on an *API 150EX* (*AB/MDS Sciex*) equipped with a Turbo Ion-Spray source. Elemental analyses were performed by *K. L. Paglia* from the Microchemical Laboratory of the University of Geneva.

3,5-Dibromo-2,4,6-trimethylpyridine (**2**).[75,76] *N*-Bromosuccinimide (NBS; 81.00 g, 0.46 mol) was added to a solution of 2,4,6-trimethylpyridine (9.00 g, 0.074 mol) and 96% H_2SO_4 (65 mL) in trifluoroacetic acid (TFA; 90 mL). The resulting solution was stirred

at 50 °C for 72 h and poured into water (200 mL) at 0 °C. The solution was basified to pH 10 with NaOH and extracted with AcOEt (4×200 mL). The organic phase was evaporated to nearly dryness. The residue was recrystallized from EtOH/H_2O (1:1) to afford **2** as a white solid (12.84 g, 62%). ^{1}H-NMR (400 MHz, $CDCl_3$): 2.61 (*s*, 6H), 2.60 (*s*, 3H). ^{13}C-NMR (400 MHz, $CDCl_3$): 154.96, 146.56, 121.21, 25.62, 24.64. ESI-MS: 277.8 ($[M+H]^+$), 279.9 ($[M+2+H]^+$), 281.8 ($[M+4+H]^+$).

3,5-Dibromo-2,6-bis(bromomethyl)-4-methylpyridine (**3**). A mixture of **2** (11.50 g, 41.22 mmol), *N*-bromosuccinimide (NBS; 29.50 g, 165.75 mmol) and azobisisobutyronitrile (AIBN; 6.80 g, 41.41 mmol) in benzene (300 mL) was refluxed for 3 h. The solution was cooled, filtered, and evaporated to dryness. THF (200 mL) was added. Diisopropylethylamine (22.26 g, 172.24 mmol) and diethyl phosphite (11.79 g, 85.39 mmol) were added at 0 °C. The solution was stirred at r.t. for 3 h. H_2O (150 mL) was added and THF was evaporated. Saturated $NaHCO_3$ (200 mL) was added, and the solution was extracted with CH_2Cl_2 (3×200 mL). The organic phase was dried over Na_2SO_4 and evaporated to dryness. The residue was purified by column chromatography (SiO_2, cyclohexane/CH_2Cl_2 100:0 to 95:5) to afford **3** as a white solid (12.15 g, 67%). ^{1}H-NMR (400 MHz, $CDCl_3$): 4.70 (*s*, 4H), 2.67 (*s*, 3H), 2.21 (*s*, 3H). ^{13}C-NMR (400 MHz, $CDCl_3$): 153.67, 149.57, 123.31, 33.61, 24.74. ESI-MS: 433.7 ($[M+H]^+$), 435.8 ($[M+2+H]^+$), 437.7 ($[M+4+H]^+$), 439.9 ($[M+6+H]^+$).

2,2′-(3,5-Dibromo-4-methylpyridine-2,6-diyl)-diacetaldehyde (**4**). A mixture of MeONa (0.56 g, 10.37 mmol) and 2-nitropropane (0.93 g, 10.47 mmol) in MeOH (100 mL) was refluxed for 30 min. Compound **3** (2.0 g., 4.58 mmol) was added at r.t. The resulting mixture was stirred at r.t. for 72 h and then evaporated to dryness. H_2O (50 mL) was added. The solution was extracted with CH_2Cl_2 (3×50 mL). The organic phase was dried over Na_2SO_4 and evaporated to dryness. The residue was purified by column chromatography (SiO_2, CH_2Cl_2/MeOH 100:1) to afford **4** as a yellow solid (0.93 g, 61%). ^{1}H-NMR (400 MHz, $CDCl_3$): 10.25 (*s*, 2H), 2.81 (*s*, 3H). ^{13}C-NMR (400 MHz, $CDCl_3$): 189.70, 152.83, 147.27, 126.83, 23.48. ESI-MS: 305.88 ($[M+H]^+$), 307.87 ($[M+2+H]^+$), 309.87 ($[M+4+H]^+$).

2,2′-(3,5-Diethenyl-4-methylpyridine-2,6-diyl)-diacetaldehyde (**5**). A mixture of **4** (0.65 g, 1.96 mmol), potassium vinyltrifluoroborate (1.32 g, 9.85 mmol), $PdCl_2$(dppf) (0.16 g, 0.20 mmol) and K_2CO_3 2 N (5.0 mL, 10.0 mmol) in toluene (50 mL) was stirred at 90 °C for 6 h. H_2O (50 mL) was added. The solution was extracted with AcOEt (3×50 mL). The organic phase was dried over Na_2SO_4 and evaporated to dryness. The residue was purified by column chromatography (SiO_2, cyclohexane/AcOEt 90:10) to afford **5** as a yellow solid (0.24 g, 62%). ^{1}H-NMR (400 MHz, CD_2Cl_2): 10.21 (*s*, 2H), 7.10 (*dd*, *J*=17.8, 11.6, 2H), 5.83 (*dd*, *J*=11.6, 1.3, 2H), 5.39 (*dd*, *J*=17.8, 1.3, 2H), 2.45 (*s*, 3H). ^{13}C-NMR (400 MHz, CD_2Cl_2): 192.94, 148.31, 147.61, 139.80, 131.55, 124.20, 17.72. ESI-MS: 202.09 ($[M+H]^+$).

4-Bromo-2-nitro-*N*-(prop-2-en-1-yl)aniline (**6**). A mixture of 4-bromo-2-nitroaniline (8.08 g, 37.23 mmol) and Cs_2CO_3 (12.14 g, 37.26 mmol) in butanone (150 mL) was stirred at 80 °C for 30 min. Allyl bromide (3.08 g, 25.42 mmol) and KI (catalytic amount) were added. The resulting mixture was stirred at 80 °C for 48 h, filtered over *Celite* and evaporated to dryness. The residue was purified by column chromatography (SiO_2, cyclohexane/CH_2Cl_2 100:0 to 80:20) to afford **6** as an orange solid (5.14 g, 79%). ^{1}H-NMR (400 MHz, $CDCl_3$): 8.33 (*d*, *J*=2.4, 1H), 8.18 (br., 1H), 7.48 (*dd*, *J*=9.2, 2.4, 1H), 6.74 (*d*, *J*=9.2, 1H), 5.92–5.88 (*m*, 1H), 5.32–5.24 (*m*, 1H), 3.99–3.95 (*m*, 2H). ^{13}C-NMR (400 MHz, $CDCl_3$): 144.28, 138.90, 132.74, 132.37, 128.92, 117.43, 115.95, 106.72, 45.38. ESI-MS: 256.9 ($[M+H]^+$), 258.9 ($[M+2+H]^+$).

4-Bromo-N^1-(prop-2-en-1-yl)benzene-1,2-diamine (**7**). A mixture of **6** (3.00 g, 11.86 mmol) and iron powder (2.60 g, 46.43 mmol) in H_2O/THF (5:1, 120 mL) was stirred at 60 °C for 12 h. The mixture was extracted with AcOEt (4×100 mL), dried over Na_2SO_4 and evaporated to dryness. The residue was purified by column chromatography (SiO_2, cyclohexane/AcOEt 80:20) to afford **7** (2.31 g, 87%) as a brown liquid. ^{1}H-NMR (400 MHz, $CDCl_3$): 6.90 (*dd*, *J*=8.4, 2.2, 1H), 6.84 (*d*, *J*=2.2, 1H), 6.50 (*d*, *J*=8.4, 1H), 6.03–5.94 (*m*, 1H), 5.32–5.26(*m*, 1H), 5.21–5.17 (*m*, 1H), 3.74 (*dt*, *J*=5.5, 1.6, 2H), 3.39 (*s*, 3H). ^{13}C-NMR (400 MHz, $CDCl_3$): 136.45, 135.89, 135.13, 123.00, 118.90, 116.63, 113.39, 110.66, 46.79. ESI-MS: 227.0 ($[M+H]^+$), 229.0 ($[M+2+H]^+$).

2,2′-(3,5-Diethenyl-4-methylpyridine-2,6-diyl)-bis[5-bromo-1-(prop-2-en-1-yl)-1*H*-1,3-benzimidazole] (**1**).[77] A mixture of **5** (0.30 g, 1.49 mmol), **7** (1.00 g, 4.40 mmol) and $Ce(NO_3)_3{\cdot}6H_2O$ (0.20 g,

0.46 mmol) in DMF (15 mL) was stirred 60 °C for 3 h. 0.01 N Na_2H_2EDTA (100 mL) was added, and the mixture was extracted with AcOEt (3×100 mL). The organic phase was washed with H_2O (2×50 mL), dried over Na_2SO_4 and evaporated to dryness. The residue was purified by column chromatography (SiO_2, CH_2Cl_2/MeOH 100:0 to 100:1) to afford **1** (0.64g, 70%) as a brown solid. ^{1}H-NMR (400 MHz, CD_2Cl_2): 7.91 (*d*, *J*=1.3, 2H), 7.41 (*dd*, *J*=8.6, 1.8, 2H), 7.29 (*d*, *J*=8.6, 2H), 6.97 (*dd*, *J*=17.8, 11.6, 2H), 8.85–5.75 (*m*, 2H), 5.45 (*dd*, *J*=11.6, 1.4, 2H), 5.19 (*dd*, *J*=17.9, 1.4, 2H), 5.08–5.06 (*m*, 2H), 4.95–4.91 (*m*, 2H), 4.80 (*dt*, *J*=5.5, 1.7, 4H), 2.51 (*s*, 3H). ^{13}C-NMR (400 MHz, CD_2Cl_2): 152.24, 146.79, 145.79, 144.50, 137.10, 134.37, 132.92, 132.63, 126.30, 123.13, 122.43, 117.98, 115.43, 112.33, 47.49, 18.54. ESI-MS: 614.06 ($[M+H]^+$), 616.05 ($[M+2+H]^+$), 618.05 ($[M+4+H]^+$).

*General Procedure for the Synthesis of [**L7**Ln(hfac)$_3$] Complexes (Ln=La, Eu, Gd, Er, Y)*

A mixture of **1** (0.10 g, 0.16 mmol, 1 equiv.) and [(dig)Ln(hfac)$_3$] (2 equiv.)[34] in CH_2ClCH_2Cl (20 mL) was stirred at r.t. for 30 min and then added to a solution of *Hoveyda-Grubbs II* (50.8 mg, 0.081 mmol, 0.5 equiv.) in CH_2ClCH_2Cl (800 mL). The resulting solution was stirred at 80 °C under N_2 for 12 h and then evaporated to dryness. The residue was purified by column chromatography (SiO_2, CH_2Cl_2/MeOH 100:0 to 100:1) and precipitation in pentane to afford [**L7**Ln(hfac)$_3$] complexes.

Data of [**L7**La(hfac)$_3$]: Yield: 59%. ^{1}H-NMR (400 MHz, CD_2Cl_2): 8.22 (*d*, *J*=1.8, 2H), 7.59 (*dd*, *J*=8.8, 1.8, 2H), 7.47 (*d*, *J*=8.8, 2H), 7.04 (*d*, *J*=10.9, 2H), 6.68 (*dt*, *J*=10.9, 6.9, 2H), 5.89 (*s*, 3H), 4.79 (*d*, *J*=6.9, 4H), 2.67 (*s*, 3H). ^{13}C-NMR (400 MHz, CD_2Cl_2): 175.85 (*q*, *J*=33.9), 151.43, 150.61, 144.73, 142.10, 133.09, 131.94, 130.06, 128.86, 128.23, 123.78, 117.61 (*q*, *J*=287.0), 117.49, 110.75, 89.88, 39.88, 17.48. ESI-MS: 1112.1 ($[M-hfac]^+$). Anal. calc. for $C_{41}H_{20}Br_2F_{18}N_5LaO_6$: C 37.33, H 1.53, N 5.31; found: C 37.29, H 1.75, N 5.21.

Data of [**L7**Eu(hfac)$_3$]. Yield: 62%. ^{1}H-NMR (400 MHz, CD_2Cl_2): 23.23 (*s*, 2H), 10.22 (*d*, *J*=8.7, 2H), 9.10 (*d*, *J*=8.8, 2H), 7.56 (*dt*, *J*=10.6 and 7.0, 2H), 6.36 (*d*, *J*=10.6, 2H), 6.25 (*d*, *J*=6.9, 4H), 3.11 (*s*, 3H). ^{13}C-NMR (400 MHz, CD_2Cl_2): 161.42, 157.28, 156.04, 149.00, 136.44, 131.82, 130.48, 127.76, 125.91, 119.35, 113.23, 106.30, 40.42, 15.83. ESI-MS: 1332.8 (M^+), 1226.2 ($[M-hfac]^+$). Anal. calc. for $C_{41}H_{20}Br_2EuF_{18}N_5O_6$: C 36.96, H 1.51, N 5.26; found: C 36.80, H 1.64, N 5.25.

Data of [**L7**Gd(hfac)$_3$]. Yield: 77%. ESI-MS: 1131.0 ($[M-hfac]^+$). Anal. calc. for $C_{41}H_{20}Br_2F_{18}GdN_5O_6$: C 36.81, H 1.51, N 5.24; found: C 36.57, H 1.63, N 5.26.

Data of [**L7**Y(hfac)$_3$]. Yield: 31%. ^{1}H-NMR (400 MHz, CD_2Cl_2): 8.32 (*d*, *J*=1.8, 2H), 7.56 (*dd*, *J*=8.8, 1.8, 2H), 7.45 (*d*, *J*=8.8, 2H), 7.04 (*d*, *J*=10.9, 2H), 6.66 (*dt*, *J*=10.9, 6.8, 2H), 5.89 (*s*, 3H), 4.81 (*d*, *J*=6.8, 4H), 2.68 (*s*, 3H). ^{13}C-NMR (101 MHz, CD_2Cl_2): 175.93 (*q*, *J*=34.1), 151.76, 150.79, 144.05, 142.45, 133.70, 131.95, 129.84, 129.34, 128.50, 125.15, 118.10 (*q*, *J*=287.6), 117.67, 110.97, 90.07, 40.41, 17.87. ESI-MS: 1062.2 ($[M-hfac]^+$). Anal. calc. for $C_{41}H_{20}Br_2F_{18}N_5O_6Y$: C 38.80, H 1.59, N 5.52; found: C 38.80, H 1.74, N 5.52.

Data of [**L7**Er(hfac)$_3$]. Yield: 16%. ESI-MS: 1141.2 ($[M-hfac]^+$). Anal. calc. for $C_{41}H_{20}Br_2ErF_{18}N_5O_6$: C 36.54, H 1.50, N 5.20; found: C 36.30, H 1.43, N 5.07.

*Synthesis of Ligand **L7** from [**L7**Ln(hfac)$_3$] Complexes (Ln=La, Eu, Gd, Er, Y)*

A mixture of [**L7**Ln(hfac)$_3$] (1 equiv.) and H_4EDTA (10 equiv.) in THF/H_2O/NH_4OH (2:2:1) was stirred at r.t. for 30 min and then extracted with CH_2Cl_2. The organic phase was dried over Na_2SO_4 and evaporated to dryness. The residue was purified by precipitation in pentane to afford ligand **L7** in 75–97% yield. ^{1}H-NMR (400 MHz, CD_2Cl_2): 8.01 (*s*, 2H), 7.47 (*d*, *J*=8.7, 2H), 7.41 (*d*, *J*=8.7, 2H), 7.01 (*d*, *J*=10.7, 2H), 6.60 (*dt*, *J*=10.3, 6.7, 2H), 4.68 (*d*, *J*=7.0, 4H), 2.56 (*s*, 3H). ^{13}C-NMR (400 MHz, CD_2Cl_2): 152.07, 146.36, 146.01, 144.63, 133.54, 130.55, 129.99, 129.65, 126.16, 123.27, 115.34, 110.71, 39.68, 16.74. ESI-MS: 558.5 ($[M+H]^+$), 560.3 ($[M+2+H]^+$), 562.1 ($[M+4+H]^+$). Anal. calc. for $C_{26}H_{17}Br_2N_5{\cdot}CH_2Cl_2$ (**L7**·CH_2Cl_2): C 50.34, H 2.97, N 10.87; found: C 50.40, H 3.23, N 11.02. The dichloromethane molecule found in the bulk solid was detected as a *singlet* at 5.32 ppm in the associated ^{1}H-NMR spectrum in $CDCl_3$ (*Figure S71*).

4-Bromo-*N*-methyl-2-nitroaniline (**8**). A mixture of 4-bromo-2-nitroaniline (13.0 g, 59.90 mmol) and Cs_2CO_3 (20.0 g, 61.38 mmol) in butanone (150 mL) was stirred at 80 °C for 30 min. CH_3I (5.70 g, 40.17 mmol) was added. The resulting mixture was stirred at 80 °C for 48 h, filtered over celite and evaporated to dryness. The residue was purified by column chromatography (SiO_2, cyclohexane/AcOEt

80:20) to afford **8** as an orange solid (8.03 g, 87%). ^{1}H-NMR (400 MHz, $CDCl_3$): 8.31 (*d*, *J* = 2.4, 1H), 8.02 (br., 1H), 7.52 (*dd*, *J* = 9.1 and 2.4, 1H), 6.76 (*d*, *J* = 9.2, 1H), 3.02 (*d*, *J* = 5.1, 3H). ^{13}C-NMR (400 MHz, $CDCl_3$): 145.24, 138.99, 132.25, 128.88, 115.13, 106.37, 29.85. ESI-MS: 231.3 ($[M+H]^+$), 233.3 ($[M+2+H]^+$).

4-Bromo-*N*^{1}-methylbenzene-1,2-diamine (**9**). A mixture of **8** (4.00 g, 17.32 mmol) and iron powder (3.90 g, 69.64 mmol) in H_2O/THF (5:1, 120 mL) was stirred at 60 °C for 12 h. The mixture was extracted with AcOEt (4×100 mL), dried over Na_2SO_4 and evaporated to dryness. The residue was purified by column chromatography (SiO_2, cyclohexane/AcOEt 80:20) to afford **9** (2.41 g, 69%) as a brown solid. ^{1}H-NMR (400 MHz, $CDCl_3$): 6.93 (*dd*, *J* = 8.4, 2.2, 1H), 6.83 (*d*, *J* = 2.2, 1H), 6.50 (*d*, *J* = 8.4, 1H), 3.34 (br., 3H), 2.83 (*s*, 3H). ^{13}C-NMR (400 MHz, $CDCl_3$): 137.90, 135.64, 123.13, 118.69, 112.22, 110.33, 30.97. ESI-MS: 201.2 ($[M+H]^+$), 203.3 ($[M+2+H]^+$).

4-Methylpyridine-2,6-dicarbaldehyde (**10**). A mixture of 2,4,6-trimethylpyridine (9.17 g, 75.66 mmol) and SeO_2 (16.80 g, 151.41 mmol) in nitrobenzene (100 mL) was stirred at 150 °C for 0.5 h. The solution was filtered over *Celite* and evaporated to dryness. The residue was purified by CC (SiO_2, cyclohexane/AcOEt 80:20) to afford **10** as white solid (1.10 g, 10%). ^{1}H-NMR (400 MHz, CD_2Cl_2): 10.15 (*s*, 2H), 7.99 (*s*, 2H), 2.55 (*s*, 3H). ^{13}C-NMR (400 MHz, CD_2Cl_2): 190.75, 151.07, 148.39, 124.18, 19.25. ESI-MS: 150.4 ($[M+H]^+$).

2,2′-(4-Methylpyridine-2,6-diyl)bis(5-bromo-1-methyl-1*H*-1,3-benzimidazole) (**L8**). A mixture of **10** (0.13 g. 0.87 mmol), **9** (0.53 g, 2.64 mmol) and $Ce(NO_3)_3{\cdot}6H_2O$ (0.19 g, 0.44 mmol) in DMF (15 mL) was stirred at 60 °C for 3 h. Na_2EDTA (1.7 g, 4.57 mmol) was added and pH was adjusted to pH 9 with NH_4OH. The mixture was stirred at r.t. for 30 min. The solution was extracted with CH_2Cl_2 (3×50 mL), dried over Na_2SO_4 and evaporated to dryness. The residue was purified by column chromatography (SiO_2, CH_2Cl_2/MeOH 100:0 to 100:1) and precipitation in pentane to afford **L8** as white solid (0.33 g, 74%). ^{1}H-NMR (400 MHz, CD_2Cl_2): 8.28 (*s*, 2H), 7.94 (*s*, 2H), 7.47 (*d*, *J* = 8.7, 2H), 7.38 (*d*, *J* = 8.6, 2H), 4.22 (*s*, 6H), 2.58 (*s*, 3H). ^{13}C-NMR (400 MHz, CD_2Cl_2): 151.42, 149.88, 149.16, 143.91, 136.37, 126.42, 126.24, 122.59, 115.37, 111.38, 32.72, 21.03. ESI-MS: 510.3 ($[M+H]^+$), 512.3 ($[M+2+H]^+$), 514.4 ($[M+4+H]^+$). Anal. calc. for $C_{22}H_{17}Br_2N_5$: C 51.69, H 3.35, N 13.70; found: C 51.55, H 3.04, N 14.19.

*General Procedure for the Synthesis of [**L8**Ln(hfac)$_3$] Complexes (Ln = La, Eu, Gd, Er, Y)*

A mixture of **L8** (1 equiv.) and [(dig)Ln(hfac)$_3$] (3 equiv.)[34] in CH_2Cl_2 was stirred at r.t. for 10 min and then evaporated to dryness. The residue was purified by SEC (*Biorad SX1*, toluene) followed by precipitation in pentane to afford [**L8**Ln(hfac)$_3$] complexes.

Data of [**L8**La(hfac)$_3$]. Yield: 71%. ^{1}H-NMR (400 MHz, CD_2Cl_2): 8.19 (*d*, *J* = 1.8, 2H), 7.91 (*s*, 2H), 7.59 (*dd*, *J* = 8.8, 1.8, 2H), 7.42 (*d*, *J* = 8.8, 2H), 5.89 (*s*, 3H), 4.17 (*s*, 6H), 2.74 (*s*, 3H). ^{13}C-NMR (400 MHz, CD_2Cl_2): 175.91 (*q*, *J* = 33.7), 153.28, 151.08, 147.92, 141.29, 135.13, 128.52, 125.40, 123.80, 119.05 (*q*, *J* = 286.7), 117.62, 111.34, 89.95, 33.26, 21.98. ESI-MS: 1271.1 (M^+), 1064.0 ($[M-hfac]^+$). Anal. calc. for $C_{37}H_{20}Br_2F_{18}LaN_5O_6$: C 34.96, H 1.59, N 5.51; found: C 35.00, H 1.65, N 5.48.

Data of [**L8**Eu(hfac)$_3$]. Yield: 73%. ^{1}H-NMR (400 MHz, CD_2Cl_2): 24.06 (*s*, 2H), 10.28 (*d*, *J* = 8.7, 2H), 9.11 (*d*, *J* = 8.7, 2H), 6.41 (*s*, 2H), 5.82 (*s*, 6H), 3.02 (*s*, 3H). ^{13}C-NMR (400 MHz, CD_2Cl_2): 159.60, 158.55, 151.14, 147.57, 136.42, 132.05, 126.02, 120.22, 113.43, 99.67, 33.13, 18.97. ESI-MS: 1078.2 ($[M-hfac]^+$). Anal. calc. for $C_{37}H_{20}Br_2F_{18}N_5O_6Eu$: C 34.60, H 1.57, N 5.45; found: C 34.60, H 1.62, N 5.39.

Data of [**L8**Gd(hfac)$_3$]. Yield: 85%. ESI-MS: 1083.3 ($[M-hfac]^+$). Anal. calc. for $C_{37}H_{20}Br_2F_{18}N_5O_6Gd$: C 34.46, H 1.56, N 5.43; found: C 34.36, H 1.67, N 5.38.

Data of [**L8**Y(hfac)$_3$]. Yield: 77%. ^{1}H-NMR (400 MHz, CD_2Cl_2): 8.30 (*d*, *J* = 1.8, 2H), 8.0 (2s, 2H), 7.56 (*dd*, *J* = 8.7 and 1.9, 2H), 7.40 (*d*, *J* = 8.7, 2H), 6.06, 5.90 (2s, 3H), 4.21 (*s*, 6H), 2.76 (3s, 3H). ESI-MS: 1014.0 ($[M-hfac]^+$). Anal. calc. for $C_{37}H_{20}Br_2F_{18}N_5O_6Y$: C 36.39, H 1.65, N 5.73; found: C 36.20, H 1.67, N 5.82.

Data of [**L8**Er(hfac)$_3$]. Yield: 79%. ESI-MS: 1093.3 ($[M-hfac]^+$). Anal. calc. for $C_{37}H_{20}Br_2ErF_{18}N_5O_6$: C 34.19, H 1.55, N 5.39; found: C 34.56, H 1.58, N 5.75.

X-Ray Crystallography

Crystals were mounted on a MiTeGen cryoloop with protection oil. Cell dimensions and intensities were

measured at 100 K or 120 K on a *Rigaku XtaLAB Synergy* diffractometer equipped with a hybrid pixel array detector (*Hypix Arc 150*) and microfocus sealed X-Ray source (Cu[Kα] radiation). The structures were solved by using dual space method with SHELXT.[78] Full-matrix least-square refinements on F^2 were performed with SHELX2014.[78] and all other calculations and drawings were performed with OLEX2[79] and ORTEP[80] programs. CCDC 2224787–2224802 contain the supplementary crystallographic data for this paper. These data are provided free of charge by the joint Cambridge Crystallographic Data Centre and Fachinformationszentrum Karlsruhe Access Structures service www.ccdc.cam.ac.uk/structures. Summary of crystal data, intensity measurements and structure refinements for ligands **1**, **L7**, **L8** and complexes [**Lk**Ln(hfac)$_3$] (**Lk** = **1**, **L7**, **L8**; Ln=La, Eu, Gd, Er, Yb, Y) and [**L7**Na(hfac)] were collected in *Tables S1–S3*, *S10*, *S13*, *S16*, *S19*, *S22*, *S29*, *S32*, *S35*, *S38*, *S41*, *S44*, *S51* and *S54*.

Supporting Information

Characterization of the new compounds are reported in the electronic supporting information which is available under https://doi.org/10.1002/hcla.202200190. CCDC deposition numbers 2224787–2224802 contain the supplementary crystallographic data for this paper. These data are provided free of charge by the joint Cambridge Crystallographic Data Centre and Fachinformationszentrum Karlsruhe Access Structure service www.ccdc.cam.ac.uk/structures.

Deposition Numbers 2224787 (for **1**), 2224788 (for [**1**Eu(hfac)$_3$]), 2224789 (for [**1**Y(hfac)$_3$]), 2224790 (for [**L7**La(hfac)$_3$]), 2224791 (for [**L7**Eu(hfac)$_3$]), 2224792 (for [**L7**Gd(hfac)$_3$]), 2224793 (for [**L7**Y(hfac)$_3$]), 2224794 (for [**L7**Er(hfac)$_3$]), 2224795 (for **L8**), 2224796 (for [**L8**La(hfac)$_3$]·CH_2Cl_2), 2224797 (for [**L8**Eu(hfac)$_3$]·2($C_5H_{12}O$)), 2224798 (for [**L8**Gd(hfac)$_3$]·2($C_4H_{10}O$)), 2224799 (for [**L8**Y(hfac)$_3$]·(CH_2Cl_2)), 2224800 (for [**L8**Er(hfac)$_3$·CH_2Cl_2]), 2224801 (for **L7**·CH_2Cl_2) and 2224802 (for [**L7**Na(hfac)]).

Acknowledgements

This work is supported through grants from the Swiss National Science Foundation (grants 200020_178758 and 200020_207313). Open Access funding provided by Université de Genève.

Data Availability Statement

The data that support the findings of this study are available from the corresponding author upon reasonable request.

Author Contribution Statement

G. L.-H. conceived the synthetic strategies, performed all the experiments and wrote the first draft of the contribution. S. N. taught and helped with the NMR titration processes and the associated thermodynamic analysis. L. G. and C. B. solved the crystal structures. C. P. conceived the whole project, got the money and wrote the final version.

References

[1] I. Kostova, 'Lanthanides as Anticancer Agents', *Curr. Med. Chem.* **2005**, *5*, 591–602.
[2] R. D. Teo, J. Termini, H. B. Gray, 'Lanthanides: Applications in Cancer Diagnosis and Therapy', *J. Med. Chem.* **2016**, *59*, 6012–6024.
[3] M. Shibasaki, N. Yoshikawa, 'Lanthanide Complexes in Multifunctional Asymmetric Catalysis', *Chem. Rev.* **2002**, *102*, 2187–2209.
[4] J.-C. G. Bünzli, 'Lanthanide Luminescent Bioprobes (LLBs)', *Chem. Lett.* **2009**, *38*, 104–109.
[5] J.-C. G. Bünzli, C. Piguet, 'Taking advantage of luminescent lanthanide ions', *Chem. Soc. Rev.* **2005**, *34*, 1048–1077.
[6] J.-F. Ayme, G. Gil-Ramírez, D. A. Leigh, J.-F. Lemonnier, A. Markevicius, C. A. Muryn, G. Zhang, 'Lanthanide Template Synthesis of a Molecular Trefoil Knot', *J. Am. Chem. Soc.* **2014**, *136*, 13142–13145.
[7] C. Lincheneau, B. Jean-Denis, T. Gunnlaugsson, 'Self-assembly formation of mechanically interlocked [2]- and [3]-catenanes using lanthanide ion Eu(III) templation and ring closing metathesis reactions', *Chem. Commun.* **2014**, *50*, 2857–2860.
[8] A. Escande, L. Guénée, K.-L. Buchwalder, C. Piguet, 'Complexation of Trivalent Lanthanides with Planar Tridentate Aromatic Ligands Tuned by Counteranions and Steric Constraints', *Inorg. Chem.* **2009**, *48*, 1132–1147.
[9] A. N. Carolan, G. M. Cockrell, N. J. Williams, G. Zhang, D. G. VanDerveer, H.-S. Lee, R. P. Thummel, R. D. Hancock, 'Selectivity of the Highly Preorganized Tetradentate Ligand 2,9-(Di(pyridi-2-yl)-1,10-phenanthroline for Metal Ions in Aqueous Solution, Including Lanthanide(III) and the Uranyl-(VI) Cation', *Inorg. Chem.* **2013**, *52*, 15–27.
[10] M. Regueiro-Figueroa, D. Esteban-Gómez, A. de Blas, T. Rodríguez-Blas, C. Platas-Iglesias, 'Understanding Stability Trends along the Lanthanide Series', *Chem. Eur. J.* **2014**, *20*, 3974–3981.
[11] R. K. Wilharm, S.-Y. Huang, I. J. Gugger, V. C. Pierre, 'A Walk Across the Lanthanide Series: Trend in Affinity for

Phosphate and Stability of Lanthanide Receptors from La(III) to Lu(III)', *Inorg. Chem.* **2021**, *60*, 15808–15817.
[12] A. Zaïm, H. Nozary, L. Guénée, C. Besnard, J.-F. Lemonnier, S. Petoud, C. Piguet, 'N-Heterocyclic Tridentate Aromatic Ligands Bound to [Ln(hexafluoroacetylacetonate)$_3$] Units: Thermodynamic, Structural and Luminescent Properties', *Chem. Eur. J.* **2012**, *18*, 7155–7168.
[13] E. Tóth, E. Brücher, 'Stability constants of the lanthanide-(III)-1,4,7,10-tetraazacyclododecane-*N*,*N*′,*N*″,*N*‴-tetraacetate complexes', *Inorg. Chim. Acta* **1994**, *221*, 165–167.
[14] A. Roca-Sabio, M. Mato-Iglesias, D. Esteban-Gómez, E. Tóth, A. de Blas, C. Platas-Iglesias, T. Rodríguez-Blas, 'Macrocyclic Receptor Exhibiting Unprecedented Selectivity of Light Lanthanides', *J. Am. Chem. Soc.* **2009**, *131*, 3331–3341.
[15] L. E. Tucker, G. C. Littman, S. Uritis, J. W. Nugent, R. P. Thummel, J. H. Reibenspies, S. B. Jones, H.-S. Lee, R. D. Hancock, 'Fluorescence and Metal-Binding Properties of the Highly Preorganized Tetradentate Ligand 2,2′-Bi-1,10-phenanthroline and Its Remarkable Affinity for Cadmium-(II)', *Inorg. Chem.* **2020**, *59*, 13117–13127.
[16] A. E. Martell, R. D. Hancock, R. J. Motekaitis, 'Factors affecting stabilities of chelate, macrocyclic and macrobicyclic complexes in solution', *Coord. Chem. Rev.* **1994**, *133*, 39–65.
[17] A. Rodríguez-Rodríguez, D. Esteban-Gómez, R. Tripier, G. Tircsó, Z. Garda, I. Tóth, A. de Blas, T. Rodríguez-Blas, C. Platas-Iglesias, 'Lanthanide(III) Complexes with a Reinforced Cyclam Ligand Show Unprecedented Kinetic Inertness', *J. Am. Chem. Soc.* **2014**, *136*, 17954–17957.
[18] P. Chen, H. Chen, P. Yan, Y. Wang, G. Li, 'Effect of lanthanide contraction and rigid ligand on the structure of salen-type lanthanide complexes', *CrystEngComm* **2011**, *13*, 6237–6242.
[19] G. M. Cockrell, G. Zhang, D. G. VanDerveer, R. P. Thummel, R. D. Hancock, 'Enhanced Metal Ion Selectivity of 2,9-Di-(pyrid-2-yl)-1,10-phenanthroline and Its Use as a Fluorescent Sensor for Cadmium(II)', *J. Am. Chem. Soc.* **2008**, *130*, 1420–1430.
[20] S. Naseri, M. Mirzakhani, C. Besnard, L. Guénée, L. Briant, H. Nozary, C. Piguet, 'Preorganized Polyaromatic Soft Terdentate Hosts for the Capture of [Ln(β-diketonate)$_3$] Guests in Solution', *Chem. Eur. J.* **2023**, *29*, e202202727.
[21] H. H. Dam, D. N. Reinhoudt, W. Verboom, 'Multicoordinate ligands for actinide/lanthanide separations', *Chem. Soc. Rev.* **2007**, *36*, 367–377.
[22] J.-H. Lan, W.-Q. Shi, L.-Y. Yuan, J. Li, Y.-L. Zhao, Z.-F. Chai, 'Recent advances in computational modeling and simulations on the An(III)/Ln(III) separation process' *Coord. Chem. Rev.* **2012**, *256*, 1406–1417.
[23] P. J. Panak, A. Geist, 'Complexation and Extraction of Trivalent Actinides and Lanthanides by Triazinylpyridine *N*-Donor Ligands', *Chem. Rev.* **2013**, *113*, 1199–1236.
[24] M. J. Hudson, L. M. Harwood, D. M. Laventine, F. W. Lewis, 'Use of Soft Heterocyclic N-Donor Ligand to Separate Actinides and Lanthanides', *Inorg. Chem.* **2013**, *52*, 3414–3428.
[25] J. Florek, S. Giret, E. Juère, D. Larivière, F. Kleitz, 'Functionalization of mesoporous materials for lanthanide and actinide extraction', *Dalton Trans.* **2016**, *45*, 14832–14854.
[26] A. Leoncini, J. Huskens, W. Verboom, 'Ligands for f-elements exctraction used in the nuclear fuel cycle', *Chem. Soc. Rev.* **2017**, *46*, 7229–7273.
[27] J. P. Sauvage, 'Interlacing Molecular Threads on Transition-Metals: Catenands, Catenates, and Knots', *Acc. Chem. Res.* **1990**, *23*, 319–327.
[28] D. H. Busch, N. A. Stephenson, 'Molecular organization, portal to supramolecular chemistry: structural-analysis of the factors associated with molecular-organization in coordination and inclusion chemistry, including the coordination template effect', *Coord. Chem. Rev.* **1990**, *100*, 119–154.
[29] M. Hutin, C. A. Schalley, G. Bernardinelli, J. R. Nitschke, 'Helicate, Macrocycle, or Catenate: Dynamic Topological Control over Subcomponent Self-Assembly', *Chem. Eur. J.* **2006**, *12*, 4069–4076.
[30] D. A. Leigh, P. J. Lusby, R. T. McBurney, A. Morelli, A. M. Z. Slawin, A. R. Thomson, D. B. Walker, 'Getting Harder: Cobalt(III)-Template Synthesis of Catenanes and Rotaxanes', *J. Am. Chem. Soc.* **2009**, *131*, 3762–3771.
[31] V. Aucagne, K. D. Hänni, D. A. Leigh, P. J. Lusby, D. B. Walker, 'Catalytic "Click" Rotaxanes: A Substoichiometric Metal-Template Pathway to Mechanically Interlocked Architectures', *J. Am. Chem. Soc.* **2006**, *128*, 2186–2187.
[32] G. Zhang, G. Gil-Ramírez, A. Markevicius, C. Browne, I. J. Vitorica-Yrezabal, D. A. Leigh, 'Lanthanide Template Synthesis of Trefoil Knots of Single Handedness', *J. Am. Chem. Soc.* **2015**, *137*, 10437–10442.
[33] M. Seitz, A. G. Oliver, K. N. Raymond, 'The Lanthanide Contraction Revisited', *J. Am. Chem. Soc.* **2007**, *129*, 11153–11160.
[34] G. Malandrino, I. L. Fragalà, 'Lanthanide "second-generation" precursors for MOCVD applications: effects of the metal ionic radius and polyether length on coordination spheres and mass-transport properties', *Coord. Chem. Rev.* **2006**, *250*, 1605–1620.
[35] S. A. Cotton, 'Establishing coordination numbers for the lanthanides in simple complexes', *C. R. Chim.* **2005**, *8*, 129–145.
[36] D. A. Leigh, L. Pirvu, F. Schaufelberger, 'Stereoselective Synthesis of Molecular Square and Granny Knots', *J. Am. Chem. Soc.* **2019**, *141*, 6054–6059.
[37] P. Martín-Ramos, M. Ramos Silva, J. T. Coutinho, L. C. J. Pereira, P. Chamorro-Posada, J. Martín-Gil, 'Single-Ion Magnetism in Luminescent Er^{3+} β-Diketonato Complex with Multiple Relaxation Mechanisms', *Eur. J. Inorg. Chem.* **2014**, 511–517.
[38] D. A. Gálico, R. Marin, G. Brunet, D. Errulat, E. Hemmer, F. A. Sigoli, J. O. Moilanen, M. Murugesu, 'Triplet-State Position and Crystal-Field Tuning in Opto-Magnetic Lanthanide Complexes: Two Sides of the Same Coin', *Chem. Eur. J.* **2019**, *25*, 14625–14637.
[39] K. Binnemans, 'Rare-earth beta-diketonate', Chapt. 225, in 'Handbook on the Physics and Chemistry of Rare Earths', Vol. 35, Eds. K. A. Geschneidner, J.-C. G. Bünzli, V. K. Pecharsky, Elsevier B. V., 2005, pp. 107–272.
[40] H. F. Brito, O. M. L. Malta, M. C. F. C. Felinto, E. E. S. Teotonio, 'Luminescence Phenomena Involving Metal Enolates', Chapt. 3, in 'The Chemistry of Metal Enolates', Wiley, 2009, pp. 131–184.

[41] Y. Hasegawa, 'Photofunctional Lanthanoid Complexes, Coordination Polymers, and Nanocrystals for Future Photonic Applications', *Bull. Chem. Soc. Jpn.* **2014**, *87*, 1029–1057.

[42] T. M. George, S. Varughese, M. L. P. Reddy, 'Near-infrared luminescence of Nd^{3+} and Yb^{3+} complexes using a polyfluorinated pyrene-based β-diketonate ligand', *RSC Adv.* **2016**, *6*, 69509–69520.

[43] J. Hayashi, S. Shoji, Y. Kitagawa, Y. Hasegawa, 'Amorphous lanthanide complexes for organic luminescent materials', *Coord. Chem. Rev.* **2022**, *467*, 214607.

[44] S. Kotha, K. Mandal, 'Suzuki-Miyaura Cross-Coupling and Ring-Closing Metathesis: A Strategic Combination for the Synthesis of Cyclophane Derivatives', *Eur. J. Org. Chem.* **2006**, 5387–5393.

[45] S. Monfette, D. E. Fogg, 'Equilibrium Ring-Closing Metathesis', *Chem. Rev.* **2009**, *109*, 3783–3816.

[46] A. Zaïm, N. Dalla Favera, L. Guénée, H. Nozary, T. N. Y. Hoang, S. V. Eliseeva, S. Petoud, C. Piguet, 'Lanthanide hexafluoroacetylacetonates *vs.* nitrates for the controlled loading of luminescent polynuclear single-stranded oligomers', *Chem. Sci.* **2013**, *4*, 1125–1136.

[47] S. Monfette, K. D. Camm, S. I. Gorelsky, D. E. Fogg, 'Electronic Effects of the Anionic Ligand in Ruthenium-Catalyzed Olefin Metathesis', *Organometallics* **2009**, *28*, 944–946.

[48] D. Casanova, J. Cirera, M. Llunell, P. Alemany, D. Avnir, S. Alvarez, 'Minimal Distortion Pathways in Polyhedral Rearrangements', *J. Am. Chem. Soc.* **2004**, *126*, 1755–1763.

[49] S. Alvarez, 'Polyhedra in (inorganic) chemistry', *Dalton Trans.* **2005**, 2209–2233.

[50] A. Ruiz-Martínez, D. Casanova, S. Alvarez, 'Polyhedral Structures with an Odd Number of Vertices: Nine-Coordinate Metal Compounds', *Chem. Eur. J.* **2008**, *14*, 1291–1303.

[51] E. A. Quadrelli, 'Lanthanide Contraction over the 4f Series Follows a Quadratic Decay', *Inorg. Chem.* **2002**, *41*, 167–169.

[52] M. Seitz, A. G. Oliver, K. N. Raymond, 'The Lanthanide Contraction Revisited', *J. Am. Chem. Soc.* **2007**, *129*, 11153–11160.

[53] G. Ferru, B. Reinhart, M. K. Bera, M. O. de la Cruz, B. Qiao, R. J. Ellis, 'The Lanthanide Contraction beyond Coordination Chemistry', *Chem. Eur. J.* **2016**, *22*, 6899–6904.

[54] I. D. Brown, 'Recent Developments in the Methods and Applications of the Bond Valence Model', *Chem. Rev.* **2009**, *109*, 6858–6919.

[55] A. Trzesowska, R. Kruszynski, T. J. Bartczak, 'New bond-valence parameters for lanthanides', *Acta Crystallogr. Sect. B* **2004**, *60*, 174–178.

[56] A. Trzesowska, R. Kruszynski, T. J. Bartczak, 'New lanthanide-nitrogen bond-valence parameters', *Acta Crystallogr. Sect. B* **2005**, *61*, 429–434.

[57] A. Trzesowska, R. Kruszynski, T. J. Bartczak, 'Bond-valence parameters of lanthanides', *Acta Crystallogr. Sect. B* **2006**, *62*, 745–753.

[58] L. Babel, T. N. Y. Hoang, L. Guénée, C. Besnard, T. A. Wesolowski, M. Humbert-Droz, C. Piguet, 'Looking for the Origin of Allosteric Cooperativity in Metallopolymers', *Chem. Eur. J.* **2016**, *22*, 8113–8123.

[59] L. Babel, L. Guénée, C. Besnard, S. V. Eliseeva, S. Petoud, C. Piguet, 'Cooperative loading of multisite receptors with lanthanide containers: an approach for organized luminescent metallopolymers', *Chem. Sci.* **2018**, *9*, 325–335.

[60] K. Baudet, V. Kale, M. Mirzakhani, L. Babel, S. Naseri, C. Besnard, H. Nozary, C. Piguet, 'Neutral Heteroleptic Lanthanide Complexes for Unravelling Host–Guest Assemblies in Organic Solvents: The Law of Mass Action Revisited', *Inorg. Chem.* **2020**, *59*, 62–75.

[61] B. M. Castellano, D. K. Eggers, 'Experimental Support for a Desolvation Energy Term in Governing Equations for Binding Equilibria', *J. Phys. Chem. B* **2013**, *117*, 8180–8188.

[62] D. K. Eggers, S. Fu, D. V. Ngo, E. H. Vuong, T. Brotin, 'Thermodynamic Contribution of Water in Cryptophane Host-Guest Binding Reaction', *J. Phys. Chem. B* **2020**, *124*, 6585–6591.

[63] M. Mirzakhani, H. Nozary, S. Naseri, C. Besnard, L. Guénée, C. Piguet, 'Bottom-Up Approach for the Rational Loading of Linear Oligomers and Polymers with Lanthanides', *Inorg. Chem.* **2021**, *60*, 15529–15542.

[64] S. W. Benson, 'Statistical Factors in the Correlation of Rate Constants and Equilibrium Constants', *J. Am. Chem. Soc.* **1958**, *80*, 5151–5154.

[65] G. Ercolani, C. Piguet, M. Borkovec, J. Hamacek, 'Symmetry Numbers and Statistical Factors in Self-Assembly and Multivalency', *J. Phys. Chem. B* **2007**, *111*, 12195–12203.

[66] G. Calzaferri, 'Entropy in multiple equilibria, theory and applications', *Phys. Chem. Chem. Phys.* **2017**, *19*, 10611–10621.

[67] C. Piguet, 'Five thermodynamic describers for addressing serendipity in the self-assembly of polynuclear complexes in solution', *Chem. Commun.* **2010**, *46*, 6209–6231.

[68] J. Hu, Q. Li, X. Wang, S. Shao, L. Wang, X. Jing, F. Wang, 'Developing Through-Space Charge Transfer as a General Approach to Realize Full-Color and White Emission with Thermally Activated Delayed Fluorescence', *Angew. Chem. Int. Ed.* **2019**, *58*, 8405–8409.

[69] A. M. Nonat, L. J. Charbonnière, 'Upconversion of light with molecular and supramolecular lanthanide complexes', *Coord. Chem. Rev.* **2020**, *409*, 213192.

[70] H. Bolvin, A. Fürstenberg, B. Golesorkhi, H. Nozary, I. Taarit, C. Piguet, 'Metal-Based Linear Light Upconversion Implemented in Molecular Complexes: Challenges and Perspectives', *Acc. Chem. Res.* **2022**, *55*, 442–456.

[71] X. Zhang, S. L. Adelman, B. T. Arko, C. R. De Silva, J. Su, S. A. Kozimor, V. Mocko, J. C. Shafer, B. W. Stein, G. Schreckenbach, E. R. Batista, P. Yang, 'Advancing the Am Extractant Design through the Interplay among Planarity, Preorganization, and Substitution Effects', *Inorg. Chem.* **2022**, *61*, 11556–11570.

[72] N. A. Thiele, D. J. Fiszbein, J. J. Woods, J. J. Wilson, 'Tuning the Separation of Light Lanthanides Using a Reverse-Size Selective Aqueous Complexant', *Inorg. Chem.* **2020**, *59*, 16522–16530.

[73] M. R. Healy, A. S. Ivanov, Y. Karslyan, V. S. Bryantsev, B. A. Moyer, S. Jansone-Popova, 'Efficient Separation of Light Lanthanides(III) by Using Bis-Lactam Phenanthroline Ligands', *Chem. Eur. J.* **2019**, *25*, 6326–6331.

[74] B. Golesorkhi, H. Nozary, A. Fürstenberg, C. Piguet, 'Erbium complexes as pioneers for implementing linear light-

upconversion in molecules', *Mater. Horiz.* **2020**, *7*, 1279–1296.
[75] N. Alsadun, G. Mouchaham, V. Guillerm, J. Czaban-Jóźwiak, A. Shkurenko, H. Jiang, P. M. Bhatt, P. Parvatkar, M. Eddaoudi, 'Introducing a Cantellation Strategy for the Design of Mesoporous Zeolite-like Metal-Organic Frameworks: Zr-sod-ZMOFs as a Case Study', *J. Am. Chem. Soc.* **2020**, *142*, 20547–20553.
[76] A.-J. Attias, C. Cavalli, B. Donnio, D. Guillon, P. Hapiot, J. Malthête, 'Columnar Mesophase from a New Disclike Mesogen Based on a 3,5-Dicyano-2,4,6-tristyrylpyridine Core', *Chem. Mater.* **2002**, *14*, 375–384.
[77] G. M. Martins, T. Puccinelli, R. A. Gariani, F. R. Xavier, C. C. Silveira, S. R. Mendes, 'Facile and efficient aerobic one-pot synthesis of benzimidazoles using $Ce(NO_3)_3{\cdot}6H_2O$ as promoter', *Tetrahedron Lett.* **2017**, *58*, 1969–1972.
[78] G. M. Sheldrick, 'Crystal structure refinement with *SHELXL*', *Acta Crystallogr. Sect. C* **2015**, *71*, 3–8.
[79] O. V. Dolomanov, L. J. Bourhis, R. J. Gildea, J. A. K. Howard, H. Puschmann, 'OLEX2: a complete structure solution, refinement and analysis program', *J. Appl. Crystallogr.* **2009**, *42*, 339–341.
[80] L. J. Farrugia, '*WinGX* and *ORTEP for Windows*: an update', *J. Appl. Crystallogr.* **2012**, *45*, 849–854.

Received December 11, 2022
Accepted February 6, 2023

